

# ASTROPHYSICS OF YOUNG STAR BINARIES

L. PRATO<sup>1,2</sup>, T. P. GREENE<sup>2,3</sup>, AND M. SIMON<sup>2,4</sup>

## ABSTRACT

This paper describes our study of the astrophysics of individual components in close pre-main-sequence binaries. We observed both stars in 17 systems, located in 4 nearby star forming regions, using low-resolution ( $R=760$ ), infrared spectroscopy and photometry. For 29 components we detected photospheric absorption lines and were able to determine spectral type, extinction,  $K$ -band excess, and luminosity. The other 5 objects displayed featureless or pure emission line spectra. In  $\sim 50\%$  of the systems, the extinction and  $K$ -band excess of the primary stars dominate those of the secondaries. Masses and ages were determined for these 29 objects by placing them on the H-R diagram, overlaid with theoretical pre-main-sequence tracks. Most of the binaries appear to be coeval. The ages span  $5 \times 10^5$  to  $1 \times 10^7$  years. The derived masses range from the sub-stellar,  $0.06 M_\odot$ , to  $2.5 M_\odot$ , and the mass ratios from  $M_2/M_1 = 0.04$  to 1.0. Fourteen stars show evidence of circumstellar disks. The  $K$ -band excess is well correlated with the  $K - L$  color for stars with circumstellar material.

## 1. Introduction

In the past decade, large numbers of young binary stars in dark cloud complexes such as Taurus and Ophiuchus have been identified (e.g., Ghez et al. 1993; Leinert et al. 1993; Reipurth & Zinnecker 1993; Simon et al. 1995). Indeed, the frequency of these multiple systems is found to be at least as great as that of the local field star population, and much higher in the case of Taurus (Duquennoy & Mayor 1991). In order to explore the astrophysics of the individual components in these multiple systems, we initiated a program to determine their properties: extinction, veiling, effective temperature ( $T_{eff}$ ), and luminosity ( $L$ ). Masses

---

<sup>1</sup>Department of Physics and Astronomy, UCLA, Los Angeles, CA 90095-1562; lprato@astro.ucla.edu

<sup>2</sup>Visiting astronomer at the Infrared Telescope Facility, which is operated by the University of Hawaii under contract from the National Aeronautics and Space Administration.

<sup>3</sup>NASA/Ames Research Center, M.S. 245-6 Moffett Field, CA 94035-1000

<sup>4</sup>Department of Physics and Astronomy, SUNY, Stony Brook, NY 11794-3800

and ages are calculated from these parameters. Mass is the most fundamental determining characteristic of a star; knowledge of masses and mass ratios in young star binaries provides insight into the binary formation mechanisms at work, and improves our understanding of the initial mass function (IMF) in these star forming clouds. Ages are important because we wish to determine if the stars in relatively close binaries are coeval in order to understand what coevality, or lack thereof, implies for models of binary star formation. Hartigan et al. (1994) found about two thirds of a sample of 26 wide ( $3'' - 45''$ ) pre-main-sequence (PMS) to be coeval. Studying a sample of closer pairs, our approach is to choose a model of PMS evolution and test the coevality of our sample on these tracks.

Brandner & Zinnecker (1997) studied 14 young binary systems, observing at visible light wavelengths. They estimated masses and ages for 8 of the systems in their sample; mass ratios ( $M_2/M_1$ ) of the components in these binaries range from 0.5 to 0.8. Kenyon & Hartigan (2001) find a wider range of mass ratios,  $\sim 0.25-1$ , in their preliminary *HST* STIS study of about a dozen PMS binaries, with separations of  $<1''$ , in the Taurus star forming region. Our approach was to study the astrophysics of young binaries in infrared (IR) rather than visible light, providing greater sensitivity to cool, red, low-mass companions and enabling the measurement of mass ratios as small as 0.04. In general, the seeing conditions are better in the near-IR in comparison to visible wavelengths, yielding improved spatial resolution for observations of close binary stars, in spite of the larger diffraction limit. The extinction is also less at longer wavelengths.

Moderate resolution *K*-band spectroscopy is useful for the characterization of young stars (Greene & Meyer 1995; Ali et al. 1996; Greene & Lada 1996; Luhman & Rieke 1998). This spectral region encompasses a variety of atomic and molecular features, such as Na I, Ca I, and the CO  $\Delta v = 2$  bandhead, which lend themselves well to the identification of G through M type stars (Luhman & Rieke 1998; Ali et al. 1996). The Br  $\gamma$  line of hydrogen serves as a surrogate diagnostic for H $\alpha$  (Prato & Simon 1997; Muzerolle et al. 1998), and the shock induced molecular hydrogen (H $_2$ ) lines across the *K*-band trace outflows in the circumstellar environment.

We obtained spectra of systems in the Taurus, Lupus, Ophiuchus, Corona Australis, and Aquila star forming regions (SFRs). We report here the results from the latter 4 regions, in which both stars in 17 systems were observed; 2 systems were observed twice. The results of the Taurus observations are in preparation (Prato et al. 2003). In §2 we describe our spectroscopic and photometric observations and data reduction. Section 3 details our approach to estimating the stellar properties for all objects with absorption line spectra. A discussion of the results is provided in §4 and the conclusions are summarized in §5. Color transformation equations and comments on individual sources appear in the Appendices.

## 2. Observations and Data Reduction

### 2.1. Observations

#### 2.1.1. Spectroscopy

The spectroscopic sample comprised 17 binary systems in the Lupus, Ophiuchus, Corona Australis, and Aquila regions with separations between  $1''.2$  and  $7''.6$ . These were selected on the basis of having separations sufficiently large to be spatially resolvable by a long slit spectrometer and brightnesses that enabled total integration times of  $<1-2$  hours in the near-IR. About half of the sample is composed of classic T Tauri stars (CTTs), i.e. systems with  $W(H\alpha) \gtrsim 10 \text{ \AA}$ ; the others are weak-lined systems (WTTs) with  $W(H\alpha) < 10 \text{ \AA}$ . Table 1 gives the object name in column (1), an alternate name in column (2), right ascension and declination in columns (3) and (4), the total  $K$ -band magnitude in column (5), the binary separation and position angle in columns (6) and (7), the year of observation in column (8), and the star forming region in column (9). Unless otherwise noted, the source of the  $K$ -band magnitude in column (5) was the photometry described in the next section. Separations and position angles were obtained from Simon et al. (1995) and Reipurth & Zinnecker (1993). With the exception of AS 353, which lies in the galactic plane, all of the SFRs studied in this project lie at galactic latitudes of  $|b| = 10^\circ - 20^\circ$ . Assuming the field star density in these regions is similar to the  $5 \times 10^{-5}$  stars per arcsecond squared found for Ophiuchus (Greene & Young 1992), there is a 5 % probability that one of the systems in our sample is not a true binary.

Fifteen spectral type standard stars were also observed. This sample consisted of nearby, main-sequence field stars with spectral types of G2V to M8V, little or no extinction, and approximately solar metallicity in most cases. Standard star properties appear in Table 2, which lists the object name in column (1), the spectral type in column (2), and the  $K$ -band magnitude in column (3). With the exception of the one subgiant in the sample, these objects and their properties were culled from an unpublished list compiled by J. Carr (private communication, 1994), derived primarily from Kirkpatrick et al. (1991) and Keenan & McNeil (1989). The subgiant, HR 8784, a G8IV, was selected from the Bright Star Catalogue (Hoffleit & Jaschek 1982).

We obtained all spectra at the University of Hawaii (UH) 2.2 m telescope in 1996 July 3, 4, and 7 (UT) and 1997 May 28 and 29 (UT), with KSPEC, the former facility near-IR spectrometer (Hodapp et al. 1994, 1996). KSPEC was equipped with a  $1024 \times 1024$  pixel HgCdTe HAWAII detector. With the telescope in its f/31 configuration, the plate scale was  $0''.167/\text{pixel}$ . By means of a prism cross-disperser, the spectral range of KSPEC spanned the

$J$ -,  $H$ - and  $K$ -bands simultaneously. Only the  $K$ -band data is used in this work since it contains the most useful variety of spectral features for characterizing extinguished, late-type young stars. The slit width for all observations was  $0''.8$ , which yielded a spectral resolution of about  $R = \lambda/\Delta\lambda = 760$ ; the slit length was  $17''$ . In most cases the stars were observed individually. In several instances, however, the spectrometer slit was aligned with both stars in a binary system and their spectra observed simultaneously. A standard beam-switch of  $6''$  along the slit was used. Exposure times varied from  $\sim 1$  to 240 s per frame. An external Argon lamp was observed to calibrate the wavelength scale. Dome flats and dark frames were also obtained.

All 1997 observations except those of WSB 28 (for want of a guide star) were made with the facility tip-tilt adaptive optics system (Pickles et al. 1994; Jim et al. 2000). Tip-tilt accomplishes a first order wavefront correction to stellar images distorted by the Earth’s atmosphere. The full width half maxima (FWHM) of the spectra for the objects measured with tip-tilt on were consistently sub-arcsecond. With tip-tilt off, the object point spread functions (PSFs) were  $\sim 1''$  wide.

### 2.1.2. Photometry

JHK photometry for most of the objects was obtained with QUIRC, the facility near-IR camera at the UH 2.2 m telescope, on 1996 July 1 (UT). Conditions were photometric. The QUIRC detector is a  $1024 \times 1024$  HgCdTe HAWAII array (Hodapp et al. 1996). In the f/31 configuration, the plate scale is  $0''.061/\text{pixel}$ . For each object at each bandpass we took 4 exposures dithered by  $7''$  to place them at 4 different positions on the array. Integration times varied from  $\sim 1$  to 45 s. Flat and dark fields were also obtained. IRAS 16231–2427, an A0 star, was observed at several different airmasses during the night in order to provide photometric calibration. Several objects were observed for which spectroscopy was not performed. The facility tip-tilt system was used for most observations.

Additional photometric measurements were made at the NASA IRTF 3m telescope in 1996 April 14 and 15 (UT) with NSFCam, the facility near-IR camera (Rayner et al. 1993; Shure et al. 1994). The conditions were photometric. NSFCam is equipped with a  $256 \times 256$  InSb detector array; observations were made at  $J$ -,  $H$ -,  $K$ -, and  $L$ - bands. The plate scale was  $0''.056/\text{pixel}$  for DoAr 24E, and  $0''.15/\text{pixel}$  for all other objects. Integration times varied from 0.1–15 s. Integration times for flat and dark frames were 0.3–2.0 s. HD 161903 (an A2 star) was observed at airmasses similar to those of the target stars for photometric calibration. Objects in Lupus, as well as AS 205 in Ophiuchus, were not observed with either QUIRC or NSFCam. For these systems, photometric data were taken from the literature

(Liu et al. 1996; Hughes et al. 1994).

## 2.2. Data Reduction

### 2.2.1. Spectroscopy

All data reduction was done with IDL routines developed by one of us (Prato 1998). A flat field was created by taking the difference of 10 median filtered flat lamp exposures and 10 median filtered dark frames. Beam-switched pairs of stellar data were differenced and divided by the final flat field. These flat-fielded, differenced frames were inspected in order to eliminate data with low signal to noise, then registered and averaged. This final average was cleaned of bad pixels by interpolation using the 4 neighboring pixels.

For those cases in which one star was observed at a time, the spectra were extracted by forming a model *K*-band PSF, averaging more than 100 individual columns in the cross-dispersion direction. By fitting the model PSF to each of the individual 1024 columns across the *K*-band and minimizing the least squares residual, weighted by the pixels with the maximum counts, the spectrum at a particular wavelength (pixel column) was extracted from the maximum value of the best-fit PSF.

If two stars with a small separation were observed simultaneously along the slit, the resulting two-dimensional spectra may overlap. In these cases, it was necessary to use a single star, observed at a similar airmass as the target binary, for creating a model point spread function. Since the binary separation and position angle were previously known (Table 1), the single star PSF was duplicated and the original and the copy superimposed at the appropriate separation to mimic the binary PSF for a particular system. The extraction procedure was analogous except that, in this case, Poisson weighting was used in fitting the model binary PSF to the observations. The binary flux ratio was determined from varying the PSF component amplitudes and finding the best fit to the data. Once the spectra were extracted, any remaining spurious bad pixels were cleaned by interpolation.

Internal reflections in the sapphire detector substrate of KSPEC gave rise to a variable frequency, interference fringing pattern across the array (Hodapp et al. 1996). To remove this pattern, the raw spectra were filtered in the Fourier domain. Differences in the equivalent widths as a result of the filtering were on the order of a few percent or less and thus significantly smaller than the uncertainties in the equivalent width measurements.

The young star and spectral standard star spectra were divided by late B or early A type stellar spectra, taken at similar airmasses, to remove atmospheric and instrumental

features. The B and A star spectra appear featureless in the  $K$ -band except for broad Br  $\gamma$  absorption lines. In order to remove this hydrogen feature, a two-part process was followed. We first interpolated over the Br  $\gamma$  line in a G dwarf spectral type standard star, and then inserted this region of the G star spectrum into the B or A star spectrum. To restore the true form of the spectrum, modified in the division by the early type telluric standard, it is necessary to multiply the final divided spectra by a  $K$ -band black body curve of temperature corresponding to the spectral type of the telluric star.

The wavelength scale was created by identifying the column positions of argon lamp lines with known wavelengths and subsequently solving for the dispersion with a 2nd order polynomial. The arc lamp column positions were identified using one 4 s exposure taken during each observing run and extracting an arc lamp spectrum from the same position on the detector where the stellar data typically fell. The sequence of reduced, wavelength calibrated spectral type standard spectra appears in Figure 1. In Figure 2, the spectra of the young binary stars are plotted.

### 2.2.2. Photometry

The QUIRC and NSFCam data were reduced in a similar manner. Successive pairs of exposures of each object were differenced for sky subtraction, flat-fielded, and cleaned of bad pixels, as for the spectroscopic data. For large separation systems, aperture photometry was obtained for the components individually. Otherwise, the photometry of the entire system was obtained and small apertures of  $0''.2$ – $0''.6$  used on the central portions of each of the binary components to determine the binary flux ratio and hence the individual magnitudes. As part of this process, airmass corrections, derived from the photometric standards, were applied.

Table 3 lists all the photometry for the complete KSPEC sample as well as for several systems for which no spectroscopic data were obtained. The first entry for each system is the primary, indicated with “A”, and the second is for the secondary object, “B”, as determined by Reipurth & Zinnecker (1993) and Simon et al. (1995). The uncertainties derive from the standard deviation of the mean of the number of counts in an aperture for a set of four or five background-subtracted exposures. In order to present the photometry on a consistent basis, we transformed from the QUIRC to the CIT systems. Details of the transformation appear in Appendix A.

Comparison of our JHK photometry with that of Greene & Young (1992), Barsony et al. (1997), and values from the *2MASS* database for objects common to our sample usually

yields results consistent to within 20 % and, in many cases, to within 5 %. For some objects, for example DoAr 24E, variations of 20–50 % were present between our photometry and that of Greene & Young (1992) and Barsony et al. (1997). However, agreement between our results for DoAr 24E and those of *2MASS* was better than  $\sim 10$  %. In general, our photometry best matched the *2MASS* data; for  $\sim 80$  % of the objects or systems in common, agreement was better than 10 %. Because T Tauri star magnitudes are known to vary considerably, these results are not surprising. The  $J - H$  and  $H - K$  colors of the stars in our sample are in good agreement, to within  $1 \sigma$ , with colors based on the photometry found in the literature (Greene & Young 1992; Barsony et al. 1997; Luhman & Rieke 1999; Koresko 2002).

### 3. Stellar Properties

#### 3.1. Color-Color Diagram

Figure 3 shows a color-color diagram based on the  $J$ -,  $H$ -, and  $K$ -band photometry from Table 3; all objects appearing in this Table are plotted except for YLW 15A (which we did not detect at  $J$ ; see Appendix B). Colors for the dwarf and giant loci are from Tokunaga (2000), transformed to the CIT photometric system. Figure 3 also shows the CTTs locus from Meyer et al. (1997). Combining the equations (5) and (6) from Greene & Meyer (1995) with the first equation in §2.2 of Meyer et al. (1997) yields

$$A_v = 13.83 (J-H)_{obs} - 8.29 (H-K)_{obs} - 7.43.$$

This derivation of  $A_v$  was used as a guide only; a quantitative treatment of the extinction appears in the next section. Using both the  $J - H$  and the  $H - K$  colors, we estimate the  $A_v$ 's of our sample, dereddening to the CTTs locus. For the WTTs in our sample, which, unextinguished, presumably lie between the CTTs and the dwarf star loci, this approach may underestimate the magnitude of the extinction, depending on the stellar spectral type.

Three stars, the primaries in Elias 2-49, AS 353, and AS 205, appear in an unexpected location,  $>1 \sigma$  below and to the right of the CTTs locus in the color-color diagram, at higher  $H - K$  and lower  $J - H$  values. One of these, Elias 2-49 A, an A1V star, is not a member of our spectroscopic sample so we will not discuss it here. Of the remaining two, AS 353 A is an unusual emission line object. In addition to  $\text{Br}\gamma$ , Na I, and CO bandhead emission, the  $2.059 \mu\text{m}$  line of He I is in emission in this object (Figure 2). Given that this is such an active source, the near-IR colors may be abnormal as a result of bound-free and free-free emission or scattering (Lada & Adams 1992). The third object in this region, the AS 205 primary, is similarly a strong  $\text{Br}\gamma$  emission line source.

### 3.2. Effective Temperature, IR Excess, and $A_v$

The observed spectra result from a combination of the young star photosphere, excess IR radiation from circumstellar disk material, IR emission from accretion processes, and interstellar extinction along the line of sight. For strong emission line objects, free-free and bound-free emission may also be present and contribute to the spectra. However, for absorption line objects with determinable spectral types, bound-free and free-free contributions to the continuum are probably negligible. Thus, we do not take these processes into account. To estimate the spectral types, IR excess, and extinction, we create model spectra of the underlying young star photosphere, beginning with an observed young star spectrum and varying the parameters of extinction, amplitude of the  $K$ -band excess, and, in some cases, the slope of this excess. We use a multi-parameter  $\chi^2$  fit to compare the modified young star spectra to spectral type template spectra. In this way, both the absorption lines and the continuum flux contribute to the determination of the spectral type,  $A_v$ , and  $K$ -band excess.

Figure 1 shows our observed library of template spectral type standard spectra. Gaps in this sequence were filled by averaging adjacent spectra: an M1.5V template was produced by averaging the M0V and M3V spectra, and an M6 was created by averaging the M5 and M7 spectra. These averaged spectra are not shown in Figure 1. Table 4 lists the wavelengths (column 1) of the spectral features for which we calculated the equivalent widths of the young stars and the template standard stars in our sample. Column (2) gives the line width used for this calculation. The species is listed in column (3), the details of the transition (Kleinmann & Hall 1986; Tokunaga 2000) in column (4), and comments in column (5). The equivalent widths measured on the basis of the parameters presented in Table 4 appear in Tables 5 and 6 for the standard template stars and the young stars, respectively.

To determine the suitability of main-sequence spectral type standards for the characterization of our young star sample, we followed the approach of Greene & Meyer (1995), illustrated in their Figure 4, and compared the positions of the standard and target stars on a plot of the Na I+Ca I *vs* CO(4–2)+CO(2–0) equivalent widths. The dwarf locus in our Figure 4 was determined from fits to the equivalent width data found in Table 5, excluding the G8IV, M7V, and M8V standards because these objects departed from a linear fit. The linear region included data from the G2.5 through the M5 standard stars. The G8IV is a sub-giant and so we did not expect it to conform to a linear fit to the dwarf standard stars. The  $1\sigma$  scatter in the dwarf star equivalent width values around the best fit line plotted in Figure 4 was  $\sim 1\text{ \AA}$ , which probably reflects some intrinsic scatter in the heterogeneous sample of standards. Hence, we characterize the uncertainty in the equivalent widths appearing in Tables 5 and 6 as  $1\text{ \AA}$ . Because the equivalent widths of many lines were detected only at

the  $1\sigma$  level, spectral type determination using line ratios was not possible (Prato 1998).

The giant star locus was defined using data from Wallace & Hinkle (1997). Digital spectra from the companion CDROM to that paper were smoothed with a Gaussian filter to reduce the spectral resolution from the original  $R \sim 5000$  to that of our KSPEC sample,  $R \sim 800$ . The resulting equivalent widths were then measured as for the dwarfs and used to determine the giant locus. In Figure 4, the distribution of the young binary stars (squares) around the dwarf locus indicates that these standards provided adequate templates for the characterization of spectral types.

To identify the young star spectral types, a procedure was used which iterated through a range of values for  $A_v$  and a constant (zero slope)  $K$ -band excess, creating several thousand modifications of each young star photospheric spectrum according to

$$f_{\text{photosphere}}(\lambda) = (f_{\text{obs}}(\lambda)e^{\tau_\lambda} - k) \times c$$

where  $f_{\text{obs}}(\lambda)$  is the observed spectrum of young star,  $\tau_\lambda = 0.92A_\lambda$ ,  $k$  is the contribution to the  $K$ -band in excess of the stellar photosphere, and  $c$  is a scaling constant which takes into account differences in the distances and radii between the spectral template standard spectrum and the model young star spectrum. To define  $A_\lambda$ , we used a linear fit to the van de Hulst no. 15 (Johnson 1968) curve between 2 and  $2.5\mu\text{m}$  and obtained a  $\lambda^{1.6}$  dependence, consistent with Rieke & Lebofsky (1985). Therefore, we define

$$A_\lambda = (0.55/\lambda(\mu\text{m}))^{1.6}A_V.$$

To first order, we approximated the  $K$ -band excess as a constant contribution across the band. We determined the values of  $A_v$  and the  $K$ -band excess by the method of least squares. For a given value of the constant,  $c$ , the  $A_v$  and  $k$  parameters were varied to minimize the residuals between the YSO spectrum and a template spectrum (Figure 1). A wide range of values for  $c$  and most of the spectral type standard stars were always tested in order to determine the best match. Visual inspection of the ten best fits of each modified young star spectrum to each standard star aided the final choice of best fit. In general, the parameters of these ten were similar and often visually indistinguishable.

For a few objects, the young star photospheric spectra could be well-fit to either an early type standard, by accounting for a large  $A_v$  with little veiling, or to a late type standard, if the value of the  $A_v$  was small but the veiling greater. In such cases, estimates of  $A_v$  from the color-color diagram (§3.1, Figure 3) were used as a guide to the most accurate fit. These objects are discussed in Appendix B.

We estimated the  $1\sigma$  uncertainties by determining at what values of  $A_v$  and  $k$  the normalized  $\chi^2 = 3.2$  (Wall 1996). Figure 5 is a contour map of  $\chi^2$  as a function of  $A_v$  and

$k$ , for a particular value of the constant  $c$  for which the  $\chi^2$  was minimized. The figure shows the fit of the modified spectrum of ROX 15 B to the M3 standard star spectrum. Standard stars of spectral types K7 to M5 were also used, but the fit to the M3 clearly produced the best apparent fit and the minimum  $\chi^2$ .

For some objects, a constant  $K$ -band excess did not produce as precise a fit to the spectral type standards as a wavelength dependent  $K$ -band excess. For these cases, we modelled the excess as a linear function of wavelength where

$$f_{\text{photosphere}}(\lambda) = (f_{\text{obs}}(\lambda)e^{\tau_\lambda} - k(\lambda)) \times c$$

and

$$k(\lambda) = m\lambda + b,$$

is the non-uniform  $K$ -band continuum excess which gives the best fit;  $m$  and  $b$  are positive constants. This applied to 5 stars, WSB 4 B, WSB 19 A, WSB 28 B, and S CrA A and B. The latter two reveal the largest  $K$ -band excesses observed in our sample. WSB 28 B is apparently substellar (§4.1); WSB 4 B and WSB 19 A are unexceptional. At wavelengths longer than  $\sim 3 \mu\text{m}$ , the IR excess is often well fit by a power law of index  $n = 0.75$  (Shu et al. 1987). However, the spectral energy distribution varies from star to star between 2 and  $3 \mu\text{m}$  (e.g. Strom et al. 1989), probably as a function of circumstellar dust temperature and the level of accretion activity. Therefore it is not surprising that we find positively sloped excesses in some cases.

Once the best values for spectral type,  $A_v$ , and  $k$  were found, the ratio of the magnitude of the  $K$ -band excess to the photospheric flux of the star at  $2.22 \mu\text{m}$ ,  $r_k = F_{K_{ex}}/F_{K_*} = k/F_{K_*}$ , was calculated. The effective YSO temperature,  $T_{\text{eff}}$ , was derived from the spectral type –  $T_{\text{eff}}$  scale illustrated in Figure 5 of Luhman (2000). Table 7 lists these derived sample properties with spectral type in column (2),  $T_{\text{eff}}$  in column (3),  $A_v$  in column (4), and  $r_k$  in column (5). For a few of the young binary components, it was not possible to determine a good fit to spectral type standards with any combination of parameters (see Appendix B). In these cases the uncertainties in spectral type were three spectral subclasses. Otherwise, typical uncertainties in spectral type were one to two spectral subclasses.

Late M star spectra are dominated by the CO bandheads, which appear at wavelengths longer than  $\sim 2.3 \mu\text{m}$  and cover about a third of the spectral region which we use for the spectral type determination described above. These features are particularly sensitive to surface gravities (Kleinmann & Hall 1986). However, because the young star targets are associated primarily with the dwarf locus in Figure 4, we are confident that low surface gravities are not effecting our results significantly. This is probably because, by the time a

star is recognizable as such, most of the contraction to the main-sequence has taken place for the systems explored here (Baraffe et al. 1998).

Paradoxically, Greene & Lada (1996) and Mamajek et al. (2002) find evidence for lower surface gravities in the  $\rho$  Ophiuchus SFR and the Sco-Cen OB complex, respectively. Although we use the same criteria here as Greene & Lada (1996), their dwarf luminosity class locus (their Figure 4) has a steeper slope than ours and was derived from a smaller sample of standard main-sequence stars. Mamajek et al. (2002) use completely different criteria for the determination of luminosity class, and, hence, surface gravities. Detailed comparisons of identical diagnostics for large samples of dwarf and giant standard stars and young stars from a variety of star forming regions with well determined ages will be necessary to understand these discrepancies.

### 3.3. Luminosity

Using  $T_{eff}$ ,  $A_v$ , and  $r_k$ , together with the  $J$ -,  $H$ - and  $K$ -band photometry, the luminosity was calculated. The procedure followed corrects the observed  $J$ -,  $H$ - and  $K$ -band magnitudes for the derived value of  $A_v$ , and the  $K$ -band magnitude for the calculated  $r_k$ . We did not correct for excess continuum emission in the  $J$ - and  $H$ -bands. At  $J$ , we assume that the excess is effectively negligible, and at  $H$ , it is typically less than half of  $r_k$  (Greene & Meyer 1995). A black body curve, determined by the stellar  $T_{eff}$ , was scaled to match the dereddened photometry. The integral under this curve provided an estimate of the luminosity, given in column (7) of Table 7.

The largest internal source of uncertainty in the final value of the luminosity derives from the distances to the SFRs under study. The values used appear in column (6) of Table 7; the references for these values appear in column (8). Unless the uncertainty was given explicitly in the reference, we used  $\pm 20$  pc. The uncertainties resulting from errors in the photometry,  $T_{eff}$ ,  $r_k$ , and  $A_v$  were smaller. Another source of error in the late M star luminosities may be attributable to the fact that the photospheres of cooler stars deviate substantially from a Planck function, depending on the metallicity (Allard et al. 1997). Thus, we could be overestimating the luminosities of the latest M stars. As a check on our estimates for the luminosities, we also followed the procedure described in Greene & Meyer (1995) for calculating luminosities from the  $J$ -band magnitudes and bolometric corrections. Our approach generally yielded larger estimates for the luminosities by a factor of 10–30 %, however, there was no trend for this discrepancy to be larger in late-type objects. The presence of unresolved companions is another source of uncertainty in the determination of luminosity; a few objects in our sample which are likely to be triples are discussed in more

detail in Appendix B.

## 4. Discussion

### 4.1. Ages, Masses, and Mass Ratios

With values for  $T_{eff}$  and luminosity from Table 7, we plot the objects in our sample on the PMS evolutionary tracks overlaid on the H-R diagram to estimate their ages and masses (Table 8). In the upper panels of Figure 6 we show the young star binary components plotted on the H-R diagram with the PMS tracks of Palla & Stahler (1999) (left) and Baraffe et al. (1998) (right). The objects cover a wide range of ages and masses, from  $\sim 1 \times 10^5$  to  $1 \times 10^7$  years and  $0.06$ – $2.5 M_{\odot}$ . They fall more completely on the younger, higher mass tracks of Palla & Stahler (1999), thus, in Figure 7, we show individual H-R diagrams for each binary pair plotted on these tracks.

Following the recommendations of Stauffer (2001), we derived  $T_{eff}$  and luminosity for a sample of 14 single, main-sequence standard stars. This sample was culled from the list of spectral type standard stars which appears in Table 2 of Prato et al. (2002). The spectral types of these objects ranged from G0 through M9. In most cases, their metallicities are solar and they are confirmed radial velocity singles. We determined their spectral types from the high-resolution  $H$ -band spectroscopy, shown in Figure 1 of Prato et al. (2002). The values of  $T_{eff}$  for the main-sequence dwarf temperature scale were obtained from Tokunaga (2000) for the G and K type standards and from Leggett et al. (2000) and Leggett et al. (2002) for the M type stars. Uncertainties in the spectral types were typically 1 subclass. The luminosities were calculated in the same way as described in §3.3. We used distances derived from the *Hipparcos* parallax, as given in the Centre de Données astronomiques de Strasbourg (SIMBAD) database, and  $J$ -,  $H$ -, and  $K$ -band magnitudes from Leggett (1992), Gezari et al. (1993), and the colors given in Tokunaga (2000) in conjunction with apparent  $V$ -band magnitudes listed in SIMBAD. Uncertainties in the luminosity reflect only uncertainties in  $T_{eff}$  and, hence, in the spectral subclass, which dominated the errors in the luminosity calculation.

In the lower panels of Figure 6 we show the positions of the 14 single, main-sequence standards described above on the H-R diagram. Isochrones only as old as  $1 \times 10^8$  years are plotted. All 14 stars fall within  $1 \sigma$  of the  $3 \times 10^7$  year isochrone on both the Palla & Stahler (1999) and Baraffe et al. (1998) tracks. This is unexpected, given that the typical ages of this main-sequence sample are thought to be  $1$ – $5 \times 10^9$  years. In general, the lower mass main-sequence stars appear to be slightly younger. In §3.3, comparison with an alternative

approach to luminosity estimates did not reveal any mass bias in our estimates of the luminosities, although in general our approach yields larger luminosities than the technique of estimating  $L$  from the bolometric correction and the  $J$ -band magnitude (Greene & Meyer 1995). A systematic overestimate of the stellar luminosities may therefore be responsible for the young ages found for the main-sequence sample on both the tracks of Baraffe et al. (1998) and those of Palla & Stahler (1999). For the stars in our PMS spectroscopic sample, this would imply underestimated ages. Alternatively, the spectral type-effective temperature conversions used for the main-sequence standards could have led to temperatures which are systematically too cool by 200–300° K.

Out of the 17 young binaries observed, it was possible to derive masses and ages for both components in 13 binaries, for one component in 3 binaries, and for neither component in the VV CrA system. Thus, we have derived masses and ages for 29 out of the 34 stars in the sample. A histogram of  $q = M_2/M_1$  for 13 systems appears in Figure 8. Although the sample is statistically small and necessarily incomplete, most of the mass ratios are distributed between  $q = 0.05$  and  $q = 0.50$ ; no concentration towards  $q = 1$  is seen, in contrast to the  $q = 1$  trend in the observed mass ratio distribution of young star spectroscopic binaries detected in visible light, illustrated in Figure 4 of Prato et al. (2002), probably the result of selection effects.

Figure 9 shows  $q$  as a function of binary separation. For the smaller separation systems, the mass ratios range from 0.04 to 1.0. However, for systems with separations greater than  $\sim 3''$ , the mass ratios are all  $< 0.3$ . Among this group of wide separation and small mass ratio systems is the WSB 28 binary, which appears to harbor a brown dwarf secondary with a mass of  $\sim 0.06 M_\odot$ . At the distance of 160 pc to Ophiuchus, the WSB 28 binary has a separation of  $\sim 800$  AU. This is consistent with the conclusions of Gizis et al. (2001) that no brown dwarf companion desert is observed at separations of 1000 AU and greater in the field star population.

Of the 13 systems with estimated ages for both components, 11 appear to be coeval within the  $1\sigma$  uncertainties. The lack of coevality in 2 of the systems, SR 21 and WSB 71, may be the outcome of faulty characterization of the component stars, the result of false binaries resulting from chance alignment, or simply statistical variations in the observed properties used to determine age. We can calculate the probability of a spurious binary in our sample in order to test the chance alignment hypothesis. With the exception of Aquila, which lies in the galactic plane, all of the SFRs studied in this project lie at galactic latitudes of  $|b| = 10^\circ - 20^\circ$ . Assuming the field star density in these regions is similar to the  $5 \times 10^{-5}$  stars per arcsecond squared found for Ophiuchus (Greene & Young 1992), there is a  $< 5\%$  probability that one of the systems in our sample is not a true binary. The

apparently non-coeval systems have two of the smallest measured mass ratios in the sample; such low mass ratio systems, if true binaries, provide good tests of the high and low-mass regimes of the tracks. Common proper motion studies of these objects would confirm or reject the premise of true binarity, improved measurements of the  $T_{eff}$ ’s and, in particular, of the luminosities, as  $\sigma(L)$  dominates the uncertainties, would reveal discrepancies in our masses and ages, and high resolution imaging would probe for higher order multiplicity. It is also possible, but more difficult to test, that in these relatively wide separation, non-coeval systems, environmental differences have played a role in their uneven development.

## 4.2. Component $A_v$ ’s

The determinations of  $A_v$  described in §3.2 and shown in Table 7 were larger than the values found from dereddening the objects to the CTTs locus in the color-color diagram (§3.1). This systematic difference may be attributable to distinct origins for the extinction measured by the two techniques. Where the color-color diagram measures the  $A_v$  to the scattering surface in a system, the spectroscopic approach measures the  $A_v$  to the stellar photosphere. Because the photosphere is typically more obscured, the spectroscopically measured  $A_v$  is larger.

Inspection of the individual  $A_v$ ’s measured for both stars in the 13 characterized systems reveals that for 6 binaries, HBC 248, WSB 28, DoAr 26, ROX 15, WSB 71, and HBC 679, the component  $A_v$ ’s do not agree within the uncertainties (Table 7). In Figure 10 we plot the primary *versus* secondary star  $A_v$ . The primary star  $A_v$ ’s are usually larger when there is a difference in the component  $A_v$ ’s. Most of the systems with different values of extinction for each component have mass ratios of  $q < 0.2$ . Large differences in component masses suggest that a higher mass primary star is associated with a deeper potential, and therefore with a larger amount of circumstellar material (Bate 2000; Prato & Monin 2001; White & Ghez 2001). This is consistent with the association of higher  $A_v$ ’s with the primary stars. White & Ghez (2001) did not observe this result in their sample of objects with  $A_v < 5$  in the Taurus star forming region. They found that the component  $A_v$ ’s tended to be similar, consistent with the results of Lada et al. (1999), which suggest a homogeneous extinction. Because our observations measure the extinction to the stellar photospheres, our results may reflect differences in the amount and distribution of circumstellar material.

### 4.3. Circumstellar Disks

#### 4.3.1. General Sample Characteristics

Dereddened  $K - L$  colors provide excellent diagnostics for the presence of circumstellar disks (Edwards et al. 1993; Prato & Simon 1997); Kenyon & Hartmann (1995) find a typical  $K - L$  variability for young stars in Taurus of only  $\sim 0.1$  mag. Edwards et al. (1993) define the presence of a circumstellar disk by a  $K - L$  color in excess of 0.2–0.4 mag. In column (3) of Table 9 we list all the  $K - L$  values available for the spectroscopic sample, compiled from this work and from the literature (see Table 3). These  $K - L$  colors range from  $\sim 0$  to 3.63. In some cases only the unresolved, systemic color was available; we include these for completeness. Before calculating the colors, the values for  $A_v$  given in Table 7 were used to deredden all of the  $K$ - and  $L$ -band magnitudes. In column (2) of Table 9 the values for the  $\text{Br}\gamma$  emission line fluxes appear. The conversion from equivalent width to line flux was performed using the dereddened  $K$ -band magnitudes.

In some cases the  $1\sigma$  uncertainties in the  $K - L$  colors are large enough that the presence of a disk is difficult to judge. For these objects, comparison with the expected photospheric colors is helpful. Results for individual objects are discussed in Appendix B. Several stars with photospheric  $K - L$  colors and small  $K$ -band excesses manifest small hydrogen emission lines. These may be chromospheric in origin (Walter et al. 1994) and are noted in column (4) of Table 9. In the four cases for which only unresolved colors are available, they are indisputably photospheric, indicating that neither component has  $K - L > 0.2$ .

Figure 11 shows the primary *versus* secondary  $K - L$  colors. No obvious correlation is present, in contrast to the results of White & Ghez (2001), however, our sample is small. A plot of primary *versus* secondary  $K$ -band excess,  $r_k$ , appears in Figure 12. In this case, a trend towards primaries with higher  $r_k$ 's than the secondaries is clear. A natural gap between low and high  $K$ -band excess occurs at  $r_k \sim 0.3$ . Below this cutoff, the excess appears negligible within the uncertainties. The trend towards higher values of primary star  $A_v$  and  $r_k$  implies the presence of more circumstellar material around the relatively more massive stars. This follows if infall onto the disks at the time of formation originated in low-angular momentum flows from a spheroidal circumbinary infall (Bate 2000).

In Figure 13 we plot  $r_k$  as a function of the  $K - L$  color for 19 individual objects. Almost every source with a large  $r_k$  also has a large  $K - L$ . Because the primary star  $r_k$  values dominate those of the secondaries (Figure 12), a predominance of primary star colors in Figure 11 is also expected. The absence of such a result probably derives from the small sample size for which both primary and secondary dereddened  $K - L$  colors are known. In Figure 13, objects with  $r_k < 0.3$  and  $K - L < 0.4$  mag are associated with little or no

circumstellar material (Edwards et al. 1993); *all objects with  $K - L < 0.4$  have  $r_k < 0.3$* . With the exception of WSB 71, stars with  $r_k > 0.3$  and  $K - L > 0.4$  mag display Br $\gamma$  line emission, indicating that these objects have active, accreting circumstellar disks.

Hydrogen emission lines vary greatly on short timescales (Graham 1992; Prato & Simon 1997) and do not always provide reliable disk diagnostics as they can give not only false positive disk detections, when in fact the emission is chromospheric in origin (Martín 1998), but also false negative results, when accretion is in quiescence. Compare, for example, the Br $\gamma$  spectra of the AS 205 and VV CrA components shown in Figure 2 of Prato & Simon (1997) and in Figure 2 of this paper. Statistically, objects with large  $K - L$  colors often have large emission line fluxes. No objects with small  $K - L$  colors are observed to have large Br $\gamma$  line fluxes, although a couple of these objects do have moderate line fluxes, probably attributable to chromospheric activity.

Using all available disk diagnostics,  $r_k$  values,  $K - L$  colors, Br $\gamma$  emission lines, and, in one case, a  $K - 12\mu\text{m}$  color, we find that 5 binaries in our sample are so-called mixed systems, in which only one component is apparently associated with circumstellar material. This is similar to the fraction of mixed systems found by Prato & Monin (2001) based on hydrogen emission lines after applying corrections for systems with marginal CTT H $\alpha$  equivalent widths and  $K - L$  colors in excess of photospheric. Of the 5 mixed systems, the two which appear to be non-coeval, SR 21 and H $\alpha$ 71, have separations of  $\gtrsim 5''$ , but the other three, WSB 4, WSB 19, and DoAr 26, have separations of  $\sim 2-3''$  (320–480 AU) and appear coeval. These three systems are puzzling; it is not obvious why stars in binaries of a few hundred AU separation which presumably formed simultaneously should manifest diverse evolutionary states. DoAr 24 E, YLW 15A, and AS 353 are yet more extreme examples of this; for these systems it was not even possible to determine the properties of one component. The geometry of these systems and the orientation of the circumstellar disks may play a role in the discrepant appearances of these binary components.

#### 4.3.2. WSB 4

The 2 $''$ 8 binary, WSB 4, displays unusual properties in the secondary star. Some confusion has propagated in the literature regarding the position angle (PA) of this pair. Zinnecker & Wilking (1992) show  $J$ -,  $H$ -,  $K$ -, and  $L$ -band images of WSB 4 (their Figure 1), however the orientation is not specified. Their Figure caption indicates that the northwest component is the optically brighter star, however, the figure itself implies a PA of  $\sim 40^\circ$ . Meyer et al. (1993) give PA =  $310^\circ$ , inconsistent with the coordinates provided for the two components in their Table 3. Reipurth & Zinnecker (1993) also list PA =  $310^\circ$ , but label the components

in their Figure 1 such that the PA  $\sim 130^\circ$ , consistent with Table 3 of Meyer et al. (1993). Koresko (2002) shows the same result. B. Reipurth (2002, private communication) verified the PA of  $130^\circ$  based on the *R*-band image shown in Reipurth & Zinnecker (1993).

Our photometry, in conjunction with the discrepancies in the literature, initially compounded the confusion because we observed that for all three bands, *J*, *H*, and *K*, the southeastern component was brighter (Table 3). Meyer et al. (1993) and Koresko (2002) both show that at wavelengths longer than  $\sim 2 \mu\text{m}$  the southeastern component is the brightest; it is also apparently significantly variable at shorter wavelengths. Because of the known variability in this system, the *K* and *L* magnitudes used to calculate the *K* – *L* colors reported for the primary and secondary in Table 9 were taken from Meyer et al. (1993). In Figures 11 and 13, the much larger, dereddened *K* – *L* color of WSB 4 B, as compared to A, stands out. WSB 4 B manifests only modest veiling, as measured by  $r_k$ . We speculate that this object might be in the process of forming an inner gap in the disk, with enough warm dust at the outer radius of this gap to give rise to the very red color (Kenyon et al. 1996). We observe a weak Br $\gamma$  emission line in WSB 4 B and Meyer et al. (1993) report an H $\alpha$  equivalent width of  $\sim 20 \text{ \AA}$ , indicating that some accretion continues to take place.

## 5. Summary

We conducted a low-resolution ( $R \sim 800$ ) *K*-band spectroscopic study of 17 angularly resolved young star binaries in the Lupus, Ophiuchus, Corona Australis, and Aquila SFRs. The spectra reveal a variety of atomic and molecular features. For 13 systems, we identified the spectral types, extinctions, and *K*-band excesses of both components, based on modelling of their photospheres and comparison with spectral type standards. These standards, also observed as part of this study, range from G2.5V to M8V. For 3 young binaries, it was only possible to identify the spectral type of one component. In the VV CrA system, neither component displayed absorption lines and thus their properties could not be identified. For those cases in which data from the literature was available for comparison, there was no obvious, systematic difference between the visible light (unresolved spatially) spectral type and our primary star spectral types.

Effective temperatures derived from spectral types and combined with near-IR photometry, usually taken at or close to the same time as most of the spectroscopic observations, yielded luminosities. All objects with assigned temperatures and luminosities were plotted on the H-R diagram overlaid with PMS evolutionary tracks. A sample of single, main-sequence stars, whose luminosities were calculated in the same way as for the young stars, show anomalously high luminosities. Thus, we suspect that our approach to the measure-

ments of the luminosity produces an overestimate by  $\lesssim 50\%$ . A spectral type-temperature conversion which causes main-sequence objects to appear to be too cool would also cause the luminosities to appear larger than expected for  $1 - 5 \times 10^9$  year old stars. Unresolved binary companions also can produce an overestimate in the luminosity. Koresko (2002) finds that several binaries in our sample appear to have sub-arcsecond companions (Appendix B).

The majority of the PMS systems are coeval on the tracks of Palla & Stahler (1999). The two that are not coeval are among the wider binaries in the sample, SR 21 and WSB 71. The mass ratios for the 13 binaries with identified properties range from 0.04 to 1. None of the mass ratios, in systems with separations  $> 3''$ , are greater than 0.3. The masses for all the stars in the sample which were assigned spectral types span  $0.06 - 2.5 M_{\odot}$ .

We examined the space density of field stars in the regions studied, with the exception of Aquila, and found that the typical probability for an interloper in one of the systems observed is  $< 5\%$ . The probability of a second interloper is negligible. Thus, the chance projection of a background star probably does not explain the non-coeval sources or the systems with very disparate components, such as DoAr 24E and AS 353. It is possible that these apparent component differences are attributable to environmental inhomogeneities and complex geometries of circumstellar material in young star binaries. This is supported by the observation that many of the systems manifest differences in the  $A_v$  of the 2 components (Table 7); in these cases, it is usually the primary star with the larger  $A_v$  (Figure 10).

Uncertainties in the distances to both the SFRs and to the individual objects within these regions comprise an important source of uncertainty in the calculation of the stellar luminosities which could effect our final results. In combination with statistical uncertainties in other observed young star properties, this might account for the 2 non-coeval pairs. In general, our approach to the calculation of the luminosity seems to produce systematic overestimates, which results in underestimates of the stellar ages.

A least half of the objects in our sample appear to have circumstellar disks. We used Br $\gamma$  emission lines,  $K - L$  colors, and  $r_k$  values as diagnostics of circumstellar material. We detected no evidence for strong dominance of primaries in a plot of secondary *versus* primary dereddened  $K - L$  colors (Figure 11), in contrast to the results of White & Ghez (2001). However, the sample for which dereddened  $K - L$  colors are known for both components is small. We do see a trend towards larger values of  $r_k$  in primaries (Figure 12); the veiling as measured by the  $K$ -band excess,  $r_k$ , may provide a better measure of circumstellar material close to the central star than the  $K - L$  color. In general, the amount of circumstellar material around the primary is expected to exceed that around the secondary star on the basis of the stronger primary star potential. Figure 13 depicts a clear correlation between large values of  $r_k$  as a function of  $K - L$  color, implying that, for stars which have high levels

of accretion, and thus a large  $r_k$ , the inner disk is optically thick, as measured by the large  $K - L$  color. One exception to this pattern is WSB 4 B; a circumstellar disk with a growing inner gap, producing a large  $K - L$  color in the absence of strong accretion, may explain this.

Five of the systems analyzed are so-called “mixed” pairs, in which only one component appears to have circumstellar material (Prato & Simon 1997; Prato & Monin 2001; Kenyon & Hartigan 2001). We used a Venn diagram analysis similar to that of Kenyon & Hartigan (2001) to compare the various disk diagnostics in the sample stars. Not all of our objects have been observed in all three diagnostics, either because the data used is incomplete, or because pure emission line spectra did not permit the calculation of  $r_k$ . However, using the existing data, we conclude that at least 17 of the objects in the sample are CTTs and no more than 17 are WTTs, some of which may reveal mid-IR excesses upon further observation (e.g., WSB 19 B). Two of the mixed pairs, WSB 71 and SR 21, are the only non-coeval binaries in the sample, and in addition have two of the largest separations. We speculate that the unmatched properties of the stars in mixed systems were determined by crucial differences in the local circumstellar environments.

YLW 15A (Figure 14) is remarkable in that it is obscured by a large  $A_v$  and is heavily veiled yet displays detectable absorption lines. This result gives us confidence that with low-resolution spectroscopy,  $R \sim 800$ , we can recover photospheric spectra veiled by as much as  $r_k = 2$ . However, higher resolution spectroscopy,  $R \gtrsim 3000$ , is far more sensitive to small absorption and emission lines (Greene & Lada 2002). This sensitivity increases with resolution. Such detailed spectroscopy can help to break the degeneracy found for some objects in our approach to estimating their properties simultaneously (§3.2) and reveal the underlying properties of more heavily veiled and obscured sources.

## 6. Acknowledgements

We thank Chris Stewart and John Dvorak of the UH 2.2 m telescope, and Dave Griep and Charlie Kaminski of the NASA IRTF for their technical support. Tracy Beck reduced the photometric data taken at the IRTF, and Saeid Zoonematkermani provided several IDL procedures used in the data reduction and helped to concatenate the panels in Figure 6 and 7; we are grateful for their assistance. Discussions with John Carr, Suzan Edwards, George Herbig, Deane Peterson, Charlie Telesco, Alycia Weinberger, and Ralph Wijers enriched this paper. We thank Russel White for providing data in advance of publication and are indebted to a meticulous, anonymous referee who provided constructive comments which

have improved this work. L. P. acknowledges generous support from Ian McLean during the preparation of this manuscript. Additional support for this work was provided by NSF grants AST 98-19694 and AST 02-05427 (to M. S.). This research has made use of the SIMBAD database, operated at CDS, Strasbourg, France. The authors wish to extend special thanks to those of Hawaiian ancestry on whose sacred mountain we are privileged to be guests.

### A. CIT Color Transformations

In order to present the QUIRC photometry in the standard CIT system, we derived a set of transformation equations based on data from Humphreys et al. (1984), Leggett et al. (1993), and Rayner (1999, private communication). We make the assumptions that (1) the color response of the QUIRC camera, with a  $1024^2$  HgCdTe HAWAII detector, on the UH 2.2 m was identical to that of the previous facility camera with a NICMOS-3 detector and, to the best of our knowledge, identical filters, and (2) that the NASA IRTF RC1 and RC2 InSb photometers also manifested identical color response to each other.

$$K_{CIT} = 0.959K_{QUIRC} + 0.041H_{QUIRC}$$

$$H_{CIT} = -0.112K_{QUIRC} + 1.112H_{QUIRC}$$

$$J_{CIT} = 0.847J_{QUIRC} + 0.360H_{QUIRC} - 0.207K_{QUIRC}$$

### B. Notes on Individual Systems

#### HBC 248

The smallest mass ratio in the sample,  $q=0.04$ , was observed in this system. Hughes et al. (1994) identified HBC 248, unresolved, as a K2, the same as our identification for the A component. We found a larger primary star  $A_v$ , 4.0 mag, than Hughes et al. (1994) detected for the pair, 1.5 mag; our estimate for the luminosity of the system is about twice as great as theirs. The secondary star  $A_v$  appears to be close to zero, differing from the primary  $A_v$  at the  $2\sigma$  level. In contrast to the results of Geoffroy & Monin (2001), our data indicate that the K2 primary and M6 secondary are coeval within the  $1\sigma$  uncertainties. Geoffroy & Monin (2001) use a fit to the spectral energy distribution to assign a secondary  $T_{eff}$  of  $\sim 4170$  K, corresponding to a K7. However, based on Figures 1 and 2, HBC 248 B appears to have a late M spectral type. The small  $K$ -band excesses in the HBC 248 components are insignificant, given the uncertainties, consistent with the small  $K - L$  color excesses (Table 9) and indicating an absence of detected circumstellar material.

## HBC 620

This system, comprised of an M0 primary and an M4.5 secondary, is coeval and appears to suffer little or no extinction. The  $K$ -band excess is effectively zero in both components, and the unresolved  $K - L$  color is photospheric. Therefore, since no color evidence for a circumstellar disk is detected, the small  $\text{Br}\gamma$  line flux present in the secondary (Table 9) is probably attributable to chromospheric activity in this late M-type star (Walter et al. 1994). Within the  $1\sigma$  uncertainties, our results for the spectral type and  $A_v$  of the primary agree with those of Hughes et al. (1994); our value for the total luminosity of the system is about 50 % greater.

## HBC 625

As in the case of HBC 620, the component stars are coeval, unextinguished, and present no significant  $K$ -band excess or  $K - L$  color excess. The primary star spectral type and lack of extinction and excess are consistent with the results of Hughes et al. (1994), although our value for the total luminosity is about twice as great. Brandner & Zinnecker (1997) list the spectral types of the stars in this system as M1 and M3, similar to our estimates of M1.5 and M4. Koresko (2002) found evidence that the secondary star in this system is actually a  $\sim 37$  milliarcsecond pair.

## AS 205

Falling on the  $1 \times 10^5$  year isochrone, the coeval components of AS 205 are among the youngest observed in this sample. Both stars are veiled, in particular the primary, and both spectra display strong  $\text{Br}\gamma$  emission lines, indicative of active accretion, and  $K - L$  colors indicative of circumstellar material. Our estimates of the AS 205 A  $A_v$  and  $L$  agree well with those of Cohen & Kuhi (1979). For the primary and secondary spectral types, Cohen & Kuhi (1979) list K0 and K5, while we find K5 and M3. Because of the large degree of veiling, these results have relatively high uncertainties. From the spectra of the VV CrA components and AS 353 A, we know that NaI and CO ca occur in emission. In conjunction with continuum veiling, line emission from hot gas partially filling in absorption line spectra could account for the greater difficulty in fitting the AS 205 spectra to standard stars. Furthermore, Koresko (2002) found that the AS 205 secondary is probably a  $\sim 9$  milliarcsecond double. This might account in part for the difficulty in fitting AS 205 B to a single, spectral type standard. Along with the emission line object, AS 353 A (Figure 2), the AS 205 primary is located more than  $1\sigma$  below the CTTs locus shown in Figure 3, possibly the result of the colors being effected by bound-free and free-free emission or scattering (Lada & Adams 1992).

## WSB 4

Please see §4.3.2 for additional details on WSB 4. We find a spectral type of M3 for both components in this coeval system, similar to the results of Martín (1998), M3 and M3.5 for the primary and secondary, respectively. Extinction is negligible along the line of sight to both stars; the south-east component, WSB 4 B, displays a small amount of veiling, indicated by a  $K$ -band excess. WSB 4 B is one of the few stars in our sample for which a linear excess with a small, positive slope yielded the best fit (§3.2).

The  $K - L$  color of WSB 4 A is within  $\sim 1 \sigma$  of photospheric, whereas the B component has a significant color excess. Martín (1998) argues that the  $20 \text{ \AA}$  equivalent width noted by Meyer et al. (1993) in WSB 4 B is attributable to chromospheric activity, and not to the classical T Tauri nature of the system. It is more probable that there is still some accretion occurring and an optically thick, circumstellar disk present around the secondary. A growing inner gap in the disk would account for the lack of IR excess at wavelengths shorter than the  $K$ -band (e.g., Haisch et al. 2001) and the relatively modest  $\text{Br}\gamma$  emission line flux.

## WSB 19

The properties we derived for the coeval components in this weak-lined system are very similar to the results of Brandner & Zinnecker (1997). In particular, values for the  $A_v$ ,  $\sim 2 - 3 \text{ mag}$ , are almost identical and the spectral types are consistent to within one and a half subclasses. The component luminosities of Brandner & Zinnecker (1997) are both about three times smaller than what we derive. Hence, although both sets of mass estimates agree well, the ages we derive are younger,  $\lesssim 1 \times 10^6$  years compared to  $\sim 3 \times 10^6$  years.

We find a significant, positively-sloped (i.e. greater at longer wavelengths)  $K$ -band excess for the primary, suggestive of circumstellar material. In the color-color diagram, WSB 19 A falls on the line between large and small near-IR excesses. This system is an IRAS source. Using the  $12 \mu\text{m}$  value for the IRAS flux density,  $0.421 \text{ Jy}$ , we find a value for the total  $K - 12\mu\text{m}$  color of  $\sim 4$ , suggestive of an optically thick, circumstellar disk at a radius of  $\lesssim 1 \text{ AU}$  (Skrutskie et al. 1990; Simon & Prato 1995) around at least the primary, given its  $K$ -band excess (Table 7). No  $L$ -band data was available for WSB 19.

## WSB 28

The M7 secondary star in WSB 28 is the lowest mass object found in our sample. From its location on the H-R diagram (Figures 6 and 7), it appears to lie below the substellar boundary. From the tracks of Palla & Stahler (1999), we obtain only an upper limit of  $0.1 M_\odot$ , however, using the Baraffe et al. (1998) tracks in Figure 6 we estimate a mass of  $0.06 M_\odot$ .

$M_{\odot}$ . There is no evidence for strong veiling,  $K - L$  excesses, or hydrogen line emission in this system, although the WSB 28 B  $K$ -band excess was found to have a linear, slightly positive slope, similar to that of WSB 4 A, but with a much smaller amplitude (by a factor of 25). The components appear to be coeval on the Baraffe et al. (1998) tracks and by extrapolation on the Palla & Stahler (1999) tracks. The binary separation,  $5''.1$ , is among the widest in the sample. The primary star is an M3.

The values from Bontemps et al. (2001) for the unresolved  $A_v$  and luminosity are 4.3 mag and  $0.36 L_{\odot}$ , respectively. We find a total luminosity of about twice this value. The primary and secondary star  $A_v$  values which we measure,  $5.1 \pm 0.6$  and  $2.5 \pm 1$ , respectively, differ both from each other and from the results of Bontemps et al. (2001).

#### DoAr 24E

DoAr 24E B is an infrared companion with no detectable photospheric features (Figure 2) and a large  $K - L$  color. In fitting the DoAr 24E A spectrum, a range of spectral types, from K0 to K2, were identified. Therefore, the designated spectral type, K0, similar to the K1 found by Luhman & Rieke (1999), is assigned a large uncertainty in Table 7. The  $A_v$ ,  $\sim 6$  mag, agrees well with values reported by Luhman & Rieke (1999) and Bontemps et al. (2001). Our  $\sim 9 L_{\odot}$  luminosity for DoAr 24E A agrees well with the  $10 L_{\odot}$  found by Luhman & Rieke (1999). The modest veiling and  $K - L$  color excess (Tables 7 and 9) imply the presence of circumstellar material around the primary, although its evolutionary stage appears to be different from that of DoAr 24E B, since the photosphere of the latter is unobservable. This discrepancy may be attributable to the geometry of this system, i.e., the secondary may be oriented such that it is observed through its optically thick disk. Data of Koresko (2002) suggest that DoAr 24E B is a  $\sim 6$  milliarcsecond pair.

Although it is not indicated in Figure 2, DoAr 24 E B appears to have weak HeI  $2.058 \mu\text{m}$  line emission of approximated the same equivalent width as its Br $\gamma$  emission line. We interpret the HeI emission as a signature of an accretion shock in optically thick gas. The excitation conditions which produce this transition are complex (Simon & Cassar 1984; Geballe et al. 1984).

#### DoAr 26

Little is known about this  $2''.3$  separation pair. We detect modest extinction towards both components,  $A_V \sim 3$  and 1 for the primary and secondary, respectively. The primary star, an M4, displays strong veiling, consistent with its location on the color-color diagram. The secondary, an M6, shows no evidence of circumstellar material. The DoAr 26 components are coeval.

## ROX 15

We find later spectral types for the coeval ROX 15 components, M3 for both, than those identified by Luhman & Rieke (1999) and Greene & Meyer (1995) for the unresolved systems, M0 in each case. Our estimates for the component  $A_v$ ’s are comparable to the unresolved values in Luhman & Rieke (1999) and Greene & Meyer (1995). Our estimate of the total luminosity,  $3.80 \pm 0.99 L_\odot$ , is consistent with that of Luhman & Rieke (1999),  $3.5 L_\odot$ . Modest veiling is observed, but no evidence of a  $K - L$  color excess or accretion activity is seen in this system.

## SR 21

The components of SR 21 do not appear to be coeval. Our estimates for the spectral type of the primary are somewhat uncertain as hydrogen emission may fill in the  $\text{Br}\gamma$  absorption line, the strongest feature in the spectrum, rendering its use problematic. Hence, we have assigned a large uncertainty to the spectral type in Table 7. The possibility of accretion activity is suggested by the strong veiling and large  $K - L$  color measured for SR 21 A. Our measurements of the  $A_v$  agree with those of Luhman & Rieke (1999) for SR 21 A, however they find a luminosity almost twice as large as ours, probably because of their much earlier spectral type, F4, estimated for the primary star. In contrast, Wilking et al. (1989) estimate a bolometric luminosity of  $7 L_\odot$ , only  $\sim 25\%$  of what we measure. The secondary star, an M4, at a separation of  $6''.4$ , appears to be unremarkable, however, it is one of the younger objects in the sample at an age of  $1 \times 10^5$  years. This may be an indication that its luminosity was overestimated. There is no evidence for circumstellar material around SR 21 B.

## YLW 15A

This is the only target in this study which is not seen at visible wavelengths. With a separation of  $7''.6$ , it is the widest binary in the sample. The  $K$ -band flux ratio of the 2 components is about 16; it was not possible to observe the secondary star at sufficiently high signal to noise to enable reliable detection of any spectral features. In the following discussion, we will use the designation YLW 15A to refer to the primary.

The spectrum of YLW 15A rises dramatically across the  $K$ -band; the appearance of very weak absorption features, and the IR nature of this source, suggest that the photosphere was observed under a large visual extinction. Although we did not detect this source in the  $J$ -band, Allen et al. (2002) observed it with the *HST*/NICMOS Camera 3 and found F110W and F160W magnitudes of  $18.22 \pm 0.16$  and  $13.05 \pm 0.01$ , respectively. Using their equations to transform to CIT  $J$ - and  $H$ -band magnitudes, we find  $J = 17.44 \pm 0.15$  mag and  $H = 12.76 \pm 0.02$  mag. Because the S/N ratio of the  $H$ -band magnitude is higher for the

data of Allen et al. (2002) than in ours, we combined these  $J$ - and  $H$ -band values together with our measurement of  $K = 9.72 \pm 0.02$ , and found an  $A_v$  of 32 mag. We note that our value of  $H$ , 14.2 mag, is significantly different from that of Allen et al. (2002), indicating an appreciable degree of veiling in this source (e.g., Greene & Lada 2002). Applying our spectral approach to finding the best values of  $A_v$ , spectral type, and  $r_k$  (measured at  $2.2 \mu\text{m}$ ) yielded 38 mag, K2, and 1.7, respectively. Given the veiling,  $r_k = 1.7$ , if we assume the presence of circumstellar material, implying that the dereddened  $K - L$  color is  $> 0.4$ , then the upper limit on the extinction is 46 mag, very close to the upper limit defined for the  $A_v$  of YLW 15A by Wilking et al. (1989) of 44 mag. Greene & Lada (2002) determined a K5 spectral type based on high resolution  $K$ -band spectroscopy. Our estimate of the luminosity of YLW 15A,  $11.4 L_\odot$ , agrees with that of Wilking et al. (1989) to within  $1 \sigma$ . Figure 14 shows the spectrum of YLW 15A after accounting for 38 magnitudes of extinction and  $r_k = 1.7$ , in comparison to a K2 spectral type standard. YLW 15A is one of the younger and more luminous sources in our sample.

## WSB 71

The components of WSB 71 provided one of the most striking examples of stars which could be well fit to a range of spectral type standards using a range of values for  $A_v$  and  $r_k$ . The uncertainties in the spectral type determination (Table 7) reflect this ambiguity. WSB 71 A, a K2, displays strong veiling. A large  $K - L$  color excess provides evidence of circumstellar material. However, only in the secondary, an M6 star, which is not veiled and shows little if any color excess, is there an emission line. This may be just the result of chromospheric activity. The total luminosity of this system,  $2.64 L_\odot$ , is consistent with that found by Greene et al. (1994),  $2.1 L_\odot$ . The stars in this system are not coeval, the primary and secondary extinctions do not agree, only one component shows evidence of a disk, and the separation is large ( $\sim 5''$ ). Proper motion studies would help to confirm this system as a true binary. Koresko (2002), using very high resolution speckle holography, found evidence for a dusty halo around the primary star. Some of the difficulty we encountered in characterizing this system may be attributable to related effects from this structure.

## S CrA

Both components of S CrA, a K3 and an M0, are strongly veiled, display large  $K - L$  colors, and have large  $\text{Br}\gamma$  line fluxes, all indicative of active accretion from circumstellar disks. A linear fit with a positive slope was necessary to define a satisfactory  $K$ -band excess. We determined a total luminosity of  $\sim 3 L_\odot$ , a somewhat lower value than that found by Wilking et al. (1992),  $5.5 L_\odot$ . The parameters for the stars are consistent; the two components appear to be coeval.

## HBC 679

HBC 679 A and B, a K5 and an M3, respectively, appear to be coeval. Neither component displays any evidence of circumstellar material. The  $A_v$  of the primary is about 2  $\sigma$  greater than that of the secondary, however, since this is a wider binary (separation  $\sim 5''$ ; 650 AU), this may be an environmental effect.

## VV CrA

When this system was observed in both 1996 and 1997, the 2 components displayed a variety of strong emission lines, including  $H_2$  in the secondary and the  $2.058 \mu\text{m}$  He I line in the primary. We observed this system twice, primarily in order to verify the He I detection. In the 1996 observations, the primary spectrum appears to display a small Ca I line in absorption. The presence of Ca I absorption in the stellar photosphere implies a spectral type of about K2 or later, consistent with the characterization of the system as a K star by Appenzeller et al. (1986). The He I emission line requires a powerful ionizing source, probably in the form of an accretion shock in optically thick gas.

The continuum flux of the secondary star appears to be varying with respect to that of the primary. For the 1996 observations, the secondary to primary flux ratio at  $2.2 \mu\text{m}$  was 1, whereas it dropped to  $\sim 0.6$  in 1997. This is consistent with the variable behavior observed in this system between 1993 and 1996 (Prato & Simon 1997).

## AS 353

As in the case of DoAr 24E, the components of the AS 353 system appear to be in distinct evolutionary stages. In this case, the primary star exhibits no absorption lines whatsoever; rather, the spectrum shows a variety of strong emission features, including the  $2.058 \mu\text{m}$  line of He I (see above discussion of DoAr 24 E and VV CrA). Repeated observations of the primary one year later (not shown in Fig. 2) produced an almost identical emission line spectrum. In contrast, the secondary component appears to be a normal, WTT M3 star with absorption lines, no veiling, and a small  $K - L$  color excess. Our spectral type for AS 353 B is later than that found by Cohen & Kuhi (1979), M0, but our estimate for  $A_v$  is equivalent to theirs within  $1\sigma$ .

The distance to this system is uncertain. Dame & Thaddeus (1985) cite  $200 \pm 100$  pc to the Aquila Rift, which provides an upper limit for the distance to the stars if we assume that the AS 353 binary is in front of the dark cloud complex. Edwards & Snell (1982) suggest a distance of 150 pc, assuming AS 353 is in Gould’s Belt. We adopt  $d = 150 \pm 50$  pc. This is consistent with a location of AS 353 B on the H-R diagram which implies an age of  $5 \times 10^5$  years for this star. Given the unremarkable appearance of this star, its young age seems

incongruous. White et al. (2003) find that AS 353 B is itself a close binary pair with an  $0''.2$  separation. If we assume a luminosity ratio of 1.0, then each component of AS 353 B has a luminosity of  $0.34 L_{\odot}$ , implying a more reasonable age of  $1 \times 10^6$  years.

Given the disparate appearance of the AS 353 components, i.e. absorption *versus* emission line spectra, and the relatively large separation,  $5''.7$ , of this system, it is possible that AS 353 is not a true binary.  $\sim 25$  background objects were observed in our  $1' \times 1'$  QUIRC field, yielding a field star density of  $\sim 7 \times 10^{-3}$  stars per square arcsecond, about 140 times greater than that measured by Greene & Young (1992) for Ophiuchus. Common proper motion measurements of the components of AS 353 would help to confirm the stars' relationship.

## REFERENCES

- Ali, B., Sellgren, K., Depoy, D. L., Carr, J. S., Gatley, I., Merrill, K. M., & Lada, E. 1997, in The X Cambridge Workshop on Cool Stars, Stellar Systems and the Sun, ASP Conf. Ser. Vol. 154, eds. R. A. Donahue and J. A. Bookbinder, p. 1663
- Allard, F., Hauschildt, P. H., Alexander, D. R., & Starrfield, S. 1997, ARA&A, 35, 137
- Allen, L. E., Myers, P. C., Di Francesco, J., Mathieu, R. D., Chen, H., & Young, E. 2002, ApJ, 566, 993
- Appenzeller, I., Jetter, R., & Jankovics, I. 1986, A&AS, 64, 65
- Baraffe, I., Chabrier, G., Allard, F., & Hauschildt, P. H. 1998, A&A, 337, 403
- Barsony, M., Kenyon, S. J., Lada, E. A., & Teuben, P. J. 1997, ApJS, 112, 109
- Bate, M. R. 2000, MNRAS, 314, 33
- Beckwith, S. V. W., Sargent, A. I., Chini, R. S., & Guesten, R. 1990, AJ, 99, 924
- Bontemps, S. 2001, A&A, 372, 173
- Brandner, W., & Zinnecker, H. 1997, A&A, 321, 220
- Calvet, N., Hartmann, L., Kenyon, S. J., & Whitney, B. A. 1994, ApJ, 434, 330
- Cohen, M., & Kuhl, L. V. 1979, ApJS, 41, 743
- Dame, T. M., & Thaddeus, P. 1985, ApJ, 297, 751
- Duquennoy, A., & Mayor, M. 1991, A&A, 248, 485

- Edwards, S., Ray, T., & Mundt, R. 1993, in *Protostars and Planets III*, ed. E. H. Levy and J. I. Lunine (Tucson: Univ. Arizona Press), 567
- Edwards, S., & Snell, R. L. 1982, *ApJ*, 261, 151
- Geballe, T. R., et al. 1984, *ApJ*, 284, 118
- Geoffray, H., & Monin, J.-L. 2001, *A&A*, 369, 239
- Gezari, D. Y., Schmitz, M., Pitts, P. S., & Mead, J. M. 1993, *Catalog of Infrared Observations (NASA RP-1294)* (3d ed.; Washington: NASA)
- Ghez, A. M., Neugebauer, G., & Matthews, K. 1995, *AJ*, 106, 2005
- Gizis, J. E., et al. 2001, *ApJ*, 551, 163
- Graham, J. A. 1992, *PASP*, 104, 479
- Greene, T. P., & Lada, C. J. 1996, *AJ*, 112, 2184
- Greene, T. P., & Lada, C. J. 2002, *AJ*, in press
- Greene, T. P., & Meyer, M. R. 1995, *ApJ*, 450, 233
- Greene, T. P., Wilking, B. A., Andre, P., Young, E. T., & Lada, C. J. 1984, *ApJ*, 434, 614
- Greene, T. P., & Young, E. T. 1992, *ApJ*, 395, 516
- Haisch, K. E., Jr., Lada, E. A., Lada, C. J. 2001, *AJ*, 121, 2065
- Hartigan, P., Strom, K. M., & Strom, S. E. 1994, *ApJ*, 427, 961
- Hodapp, K.-W., Hora, J. L., Irwin, E., & Young, T. 1994, *PASP*, 106, 87
- Hodapp, K.-W., et al. 1996, *New Astron.*, 1, 177
- Hoffleit, D., & Jaschek, C. 1982, *The Bright Star Catalogue* (4th rev. ed.; New Haven: Yale Univ. Obs.)
- Hughes, J., Hartigan, P., Krautter, J., & Kelemen, J. 1994, *AJ*, 108, 1071
- Humphreys, R. M., Jones, T. J., & Sitko, M. L. 1984, *AJ*, 89, 1155
- Jim, K. T. C., et al. 2000, *PASP*, 112, 716

- Johnson, H. L. 1968, in *Nebulae and Interstellar Matter*, ed. B. M. Middlehurst and L. H. Aller (Chicago: University of Chicago Press), p. 167
- Keenan, P. C., & McNeil, R. C. 1989, *ApJS*, 71, 245
- Kenyon, S. J., & Hartigan, P. 2001, *IAU Symp.* 200, The Formation of Binary Stars, 323
- Kenyon, S. J., & Hartmann, L. 1995, *ApJS*, 101, 117
- Kenyon, S. J., Yi, I., & Hartmann, L. 1996, *ApJ*, 462, 439
- Kirkpatrick, J. D., Henry, T. J., & McCarthy, D. W., Jr. 1991, *ApJS*, 77, 417
- Kleinmann, S. G., & Hall, D. N. B. 1986, *ApJS*, 62, 501
- Koresko, C. D., Herbst, T. M., & Leinert, Ch. 1997, *ApJ*, 480, 741
- Koresko, C. D. 2002, *AJ*, 124, 1082
- Lada, C. J., & Adams, F. C. 1992, *ApJ*, 393, 278
- Lada, C. J., Alves, J., & Lada, E. A. 1999, *ApJ*, 512, 250
- Leggett, S. K. 1992, *ApJS*, 82, 351
- Leggett, S. K., Allard, F., Dahn, Conard, Hauschildt, P. H., Kerr, T. H., & Rayner, J. 2000, *ApJ*, 535, 965
- Leggett, S. K., et al. 2002, *ApJ*, 564, 452
- Leggett, S. K., Smith, J. A., & Oswalt, T. D. 1993, in *IAU Colloq.* 136, *Stellar Photometry - Current Techniques and Future Developments*, ed. C.J. Butler and I. Elliott (Cambridge: Cambridge Univ. Press), p. 66
- Leinert, Ch., Zinnecker, H., Weitzel, N., Christou, J., Ridgway, S. T., Jameson, R., Haas, M., & Lenzen, R. 1993, *A&A*, 278, 129
- Liu, M. C., et al. 1996, *ApJ*, 461, 334
- Luhman, K. L., & Rieke, G. H. 1998, *ApJ*, 497, 354
- Luhman, K. L., & Rieke, G. H. 1999, *ApJ*, 525, 440
- Luhman, K. L. 2000, *ApJ*, 544, 1044
- Mamajek, E. E., Meyer, M. R., & Leibert, J. W. 2002, *AJ*, 124, 1670

- Martín, E. L. 1998, *AJ*, 115, 351
- Meyer, M. R., Wilking, B. A., & Zinnecker, H. 1993, *AJ*, 105, 619
- Meyer, M. R., Calvet, N., & Hillenbrand, L. A. 1997, *AJ*, 114, 288
- Mundt, R., Stocke, J., & Stockman, H. S. 1983, *ApJ*, 265, L71
- Muzerolle, J., Hartmann, L., & Calvet, N. 1998, *AJ*, 116, 2965
- Palla, F., & Stahler, S. W. 1999, *ApJ*, 525, 772
- Pickles, A. J., et al. 1994, *SPIE*, 2199, 504
- Prato, L. 1998, Ph.D. Thesis, SUNY Stony Brook
- Prato, L., & Monin, J.-L. 2001, *IAU Symp.* 200, The Formation of Binary Stars, 313
- Prato, L., & Simon, M. 1997, *ApJ*, 474, 455
- Prato, L., Simon, M., Mazeh, T., McLean, I. S., Norman, D., & Zucker, S. 2002, *ApJ*, 569, 863
- Rayner, J. T., et al. 1993, *SPIE*, 1946, 490
- Reipurth, B., & Zinnecker, H. 1993, *A&A*, 278, 81
- Rieke, G. H., & Lebofsky, M. J. 1985, *ApJ*, 288, 618
- Shu, F. H., Adams, F. C., & Lizano, S. 1987, *ARA&A*, 25, 23
- Shure, M. A., Toomey, D. W., Rayner, J. T., Onaka, P. M., & Denault, A. J. 1994, *SPIE*, 2198, 614
- Simon, M., & Cassar, L. 1984, *ApJ*, 283, 179
- Simon, M., et al. 1995, *ApJ*, 443, 625
- Simon, M., & Prato, L. 1995, *ApJ*, 450, 824
- Skrutskie, M. F., Dutkevitch, D., Strom, S. E., Edwards, S., Strom, K. M., & Shure, M. A. 1990, *AJ*, 99, 1187
- Stauffer, J. R. 2001, in *Young Stars Near Earth: Progress and Prospects*, San Francisco: ASP Conf. Series, Vol. 244, ed. R. Jayawardhana and T. Greene, p. 127

- Strom, K. M., Strom, S. E., Edwards, S., Cabrit, S., & Skrutskie, M. F. 1989, *AJ*, 97, 1451
- Tokunaga, A. T. 2000, in *Astrophysical Quantities*, ed. A. N. Cox (New York: Springer-Verlag), 143
- Torres, G., & Ribas, I. 2002, *ApJ*, 567, 1140
- Wall, J. V. 1996, *QJRAS*, 37, 519
- Wallace, L., & Hinkle, K. 1997, *ApJS*, 111, 445
- Walter, F.M., Vrba, F. J., Mathieu, R. D., Brown, A., & Myers, P. C. 1994, *AJ*, 107, 692
- Walter, F.M., Vrba, F. J., Wolk, S. J., Mathieu, R. D., & Neuhauser, R. 1997, *AJ*, 114, 1544
- White, R. J., et al., in preparation
- White, R. J., & Ghez, A. M. 2001, *ApJ*, 556, 265
- Wilking, B. A., Greene, T. P., Lada, C. J., Meyer, M. R., & Young, E. T. 1992, *ApJ*, 397, 520
- Wilking, B. A., Lada, C. J., & Young, E. T. 1989, *ApJ*, 340, 823
- Zinnecker, H., & Wilking, B. A. 1992, in *Proceedings of a Workshop held in Bettmeralp, Switzerland, Sept. 1991, Binaries as Tracers of Stellar Formation*, ed. A. Duquennoy & M. Mayor (Cambridge: Cambridge University Press), 269

Table 1. Spectroscopic Sample

| Source Name(s) |               | R.A.<br>(J2000.0) | Decl.<br>(J2000.0) | $K$<br>(mag)      | Sep.<br>( $''$ ) | P.A.<br>( $^{\circ}$ ) | Year<br>Observed | SFR  |
|----------------|---------------|-------------------|--------------------|-------------------|------------------|------------------------|------------------|------|
| HBC 248        | Sz 68         | 15 45 12.9        | −34 17 30.6        | 6.52 <sup>a</sup> | 2.6              | 295                    | 1997             | Lup  |
| HBC 620        | Sz 108        | 16 08 42.7        | −39 06 18.3        | 8.63 <sup>a</sup> | 4.2              | 25                     | 1997             | Lup  |
| HBC 625        | Sz 116        | 16 09 42.6        | −39 19 42.0        | 9.48 <sup>a</sup> | 1.5              | 29                     | 1997             | Lup  |
| AS 205         | HBC 254       | 16 11 31.40       | −18 38 24.5        | 5.54 <sup>b</sup> | 1.3              | 204                    | 1996             | Oph  |
| WSB 4          | ...           | 16 18 50.3        | −26 10 08.0        | 9.59              | 2.8              | 129                    | 1997             | Oph  |
| WSB 19         | ...           | 16 25 02.2        | −24 59 31.0        | 9.12              | 1.5              | 264                    | 1997             | Oph  |
| WSB 28         | ISO−Oph 27    | 16 26 20.7        | −24 08 48.0        | 9.38              | 5.1              | 358                    | 1997             | Oph  |
| DoAr 24E       | HBC 639       | 16 26 23.4        | −24 21 02.0        | 6.7               | 2.2              | 150                    | 1996             | Oph  |
| DoAr 26        | WSB 35        | 16 26 34.8        | −23 45 41.0        | 8.89              | 2.3              | 132                    | 1996             | Oph  |
| ROX 15         | Elias 2-26    | 16 26 42.9        | −24 20 32.0        | 8.00              | 1.2              | 70                     | 1996             | Oph  |
| SR 21          | YLW 8         | 16 27 10.2        | −24 19 16.0        | 6.35              | 6.4              | 175                    | 1996             | Oph  |
| YLW 15A        | ISO−Oph 141   | 16 27 27.1        | −24 40 51.0        | 9.65              | 7.6              | 21                     | 1997             | Oph  |
| WSB 71         | H $\alpha$ 71 | 16 31 30.9        | −24 24 40.0        | 8.1               | 4.8              | 40                     | 1996             | Oph  |
| S CrA          | HBC 286       | 19 01 08.7        | −36 57 19.8        | 6.08              | 1.3              | 160                    | 1996             | CrA  |
| HBC 679        | WaCrA3        | 19 02 22.4        | −36 55 41.0        | 9.09              | 4.5              | 60                     | 1996             | CrA  |
| VV CrA         | HBC 291       | 19 03 06.7        | −37 12 51.0        | 6.49              | 1.9              | 45                     | 1996, 1997       | CrA  |
| AS 353         | HBC 292       | 19 20 31.0        | +11 01 54.9        | 7.73              | 5.7              | 175                    | 1996             | L673 |

Note. — Units of right ascension are hours, minutes, and seconds, and units of declination are degrees, arcminutes, and arcseconds.

<sup>a</sup>Hughes et al. 1994

<sup>b</sup>Liu et al. 1996

Table 2. Spectral Type Standards

| Name     | Spectral Type | $K$<br>(mag) |
|----------|---------------|--------------|
| HR 88    | G2.5 V        | 4.9          |
| HR 8631  | G4 V          | 4.2          |
| HR 9088  | G5 Vb         | 4.2          |
| HR 8784  | G8 IV         | 4.6          |
| HR 166   | K0 V          | 4.0          |
| GL 28    | K2 V          | 5.1          |
| HR 8832  | K3 V          | 3.1          |
| HR 8085  | K5 V          | 2.4          |
| HR 8086  | K7 V          | 2.9          |
| GL 763   | M0 V          | 5.9          |
| GL 752A  | M3 V          | 4.7          |
| GL 791.2 | M4.5 V        | 7.3          |
| GL 83.1  | M5 V          | 6.7          |
| GL 644C  | M7 V          | 8.8          |
| GL 752B  | M8 V          | 8.8          |

Table 3. Component Resolved Photometry

| Name                  |   | $J$<br>(mag)     | $H$<br>(mag)     | $K$<br>(mag)     | $L$<br>(mag)                | References<br>( $L$ -band) |
|-----------------------|---|------------------|------------------|------------------|-----------------------------|----------------------------|
| HBC 248 <sup>a</sup>  | A | $7.67 \pm 0.03$  | $6.96 \pm 0.08$  | $6.62 \pm 0.09$  | $6.07 \pm 0.05$             | 1                          |
|                       | B | $10.58 \pm 0.03$ | $9.78 \pm 0.10$  | $9.29 \pm 0.09$  | $8.81 \pm 0.08$             | 1                          |
| HBC 620 <sup>a</sup>  | A | $9.76 \pm 0.02$  | $9.09 \pm 0.02$  | $8.78 \pm 0.01$  | $L_{total} = 8.48 \pm 0.01$ | 2                          |
|                       | B | $12.02 \pm 0.04$ | $11.21 \pm 0.03$ | $10.86 \pm 0.03$ |                             |                            |
| HBC 625 <sup>a</sup>  | A | $10.84 \pm 0.03$ | $10.13 \pm 0.01$ | $9.91 \pm 0.02$  | $L_{total} = 9.36 \pm 0.02$ | 2                          |
|                       | B | $11.48 \pm 0.03$ | $10.90 \pm 0.01$ | $10.71 \pm 0.02$ |                             |                            |
| AS 205 <sup>b</sup>   | A | $8.15 \pm 0.06$  | $7.16 \pm 0.06$  | $5.90 \pm 0.03$  | $4.9 \pm 0.1$               | 3, 4                       |
|                       | B | $9.24 \pm 0.17$  | $7.97 \pm 0.13$  | $6.90 \pm 0.14$  | $5.8 \pm 0.1$               | 3, 4                       |
| WSB 4                 | A | $11.70 \pm 0.06$ | $10.96 \pm 0.04$ | $10.63 \pm 0.06$ | $9.50 \pm 0.12$             | 5                          |
|                       | B | $11.55 \pm 0.06$ | $10.69 \pm 0.03$ | $10.12 \pm 0.06$ | $10.21 \pm 0.12$            | 5                          |
| WSB 18 <sup>c</sup>   | A | $11.47 \pm 0.05$ | $10.48 \pm 0.03$ | $10.01 \pm 0.06$ | ...                         |                            |
|                       | B | $12.18 \pm 0.06$ | $11.11 \pm 0.03$ | $10.34 \pm 0.06$ | ...                         |                            |
| WSB 19                | A | $11.16 \pm 0.03$ | $10.13 \pm 0.04$ | $9.53 \pm 0.15$  | ...                         |                            |
|                       | B | $11.76 \pm 0.04$ | $10.85 \pm 0.04$ | $10.38 \pm 0.16$ | ...                         |                            |
| HBC 257 <sup>c</sup>  | A | $9.45 \pm 0.07$  | $8.46 \pm 0.03$  | $7.86 \pm 0.09$  | ...                         |                            |
|                       | B | $10.17 \pm 0.08$ | $9.29 \pm 0.05$  | $8.89 \pm 0.12$  | ...                         |                            |
| WSB 26 <sup>c</sup>   | A | $11.45 \pm 0.06$ | $10.45 \pm 0.04$ | $9.46 \pm 0.08$  | ...                         |                            |
|                       | B | $11.63 \pm 0.06$ | $10.46 \pm 0.04$ | $9.78 \pm 0.08$  | ...                         |                            |
| WSB 28                | A | $10.89 \pm 0.06$ | $9.82 \pm 0.03$  | $9.48 \pm 0.07$  | ...                         |                            |
|                       | B | $13.41 \pm 0.18$ | $12.37 \pm 0.11$ | $11.84 \pm 0.18$ | ...                         |                            |
| DoAr 24E <sup>d</sup> | A | $9.2 \pm 0.3$    | $7.8 \pm 0.2$    | $7.1 \pm 0.1$    | $6.43 \pm 0.07$             | 6                          |
|                       | B | $12.1 \pm 0.4$   | $9.7 \pm 0.2$    | $8.1 \pm 0.1$    | $5.9 \pm 0.1$               | 6                          |
| DoAr 26               | A | $11.17 \pm 0.07$ | $9.98 \pm 0.04$  | $9.17 \pm 0.06$  | ...                         |                            |
|                       | B | $11.83 \pm 0.09$ | $10.98 \pm 0.07$ | $10.56 \pm 0.08$ | ...                         |                            |
| ROX 15                | A | $10.70 \pm 0.04$ | $9.19 \pm 0.05$  | $8.29 \pm 0.05$  | $L_{total} = 7.09 \pm 0.10$ | 7                          |
|                       | B | $12.20 \pm 0.07$ | $10.57 \pm 0.09$ | $9.66 \pm 0.07$  |                             |                            |
| SR 21 <sup>d</sup>    | A | $8.77 \pm 0.02$  | $7.45 \pm 0.04$  | $6.40 \pm 0.03$  | $5.25 \pm 0.03$             | 6                          |
|                       | B | $12.03 \pm 0.04$ | $10.54 \pm 0.03$ | $9.70 \pm 0.02$  | $9.26 \pm 0.04$             | 6                          |
| YLW 15A <sup>d</sup>  | A | ...              | $14.2 \pm 0.1$   | $9.72 \pm 0.02$  | $6.70 \pm 0.01$             | 6                          |
|                       | B | ...              | $15.7 \pm 0.2$   | $12.69 \pm 0.06$ | $11.0 \pm 0.5$              | 6                          |

Table 3—Continued

| Name                    |   | $J$<br>(mag)     | $H$<br>(mag)     | $K$<br>(mag)     | $L$<br>(mag)                | References<br>( $L$ -band) |
|-------------------------|---|------------------|------------------|------------------|-----------------------------|----------------------------|
| WSB 71 <sup>d</sup>     | A | $11.00 \pm 0.03$ | $9.50 \pm 0.03$  | $8.3 \pm 0.2$    | $6.67 \pm 0.01$             | 6                          |
|                         | B | $11.4 \pm 0.2$   | $10.34 \pm 0.2$  | $10.0 \pm 0.2$   | $9.17 \pm 0.04$             | 6                          |
| Elias 2-49 <sup>c</sup> | A | $6.99 \pm 0.03$  | $6.18 \pm 0.05$  | $5.32 \pm 0.04$  | ...                         |                            |
|                         | B | $9.00 \pm 0.09$  | $8.14 \pm 0.12$  | $7.73 \pm 0.10$  | ...                         |                            |
| S CrA                   | A | $8.60 \pm 0.04$  | $7.50 \pm 0.05$  | $6.56 \pm 0.06$  | $5.06^e$                    | 2, 9                       |
|                         | B | $9.37 \pm 0.06$  | $8.28 \pm 0.08$  | $7.27 \pm 0.08$  | $6.07^e$                    | 2, 9                       |
| HBC 679                 | A | $10.37 \pm 0.03$ | $9.50 \pm 0.04$  | $9.24 \pm 0.06$  | $L_{total} = 9.12 \pm 0.04$ | 10                         |
|                         | B | $12.48 \pm 0.07$ | $11.56 \pm 0.06$ | $11.18 \pm 0.08$ |                             |                            |
| VV CrA                  | A | $9.60 \pm 0.05$  | $8.38 \pm 0.05$  | $7.27 \pm 0.05$  | $6.28 \pm 0.04$             | 2, 11                      |
|                         | B | $12.07 \pm 0.22$ | $9.69 \pm 0.08$  | $7.33 \pm 0.05$  | $3.70 \pm 0.04$             | 2, 11                      |
| AS 353                  | A | $10.03 \pm 0.03$ | $9.16 \pm 0.02$  | $8.23 \pm 0.03$  | $6.35 \pm 0.01$             | 8                          |
|                         | B | $10.22 \pm 0.04$ | $9.20 \pm 0.04$  | $8.76 \pm 0.04$  | $8.21 \pm 0.08$             | 8                          |

Note. — All  $J$ -,  $H$ -, and  $K$ -band QUIRC and IRTF photometry is presented in the CIT system.

<sup>a</sup> $J$ -,  $H$ -, and  $K$ -band photometry from Hughes et al. (1994)

<sup>b</sup> $J$ -,  $H$ -, and  $K$ -band photometry from Liu et al. (1996)

<sup>c</sup>Not members of the spectroscopic sample.

<sup>d</sup>Photometry from IRTF.

<sup>e</sup>No uncertainty was given in the references.

References. — (1) Geoffray & Monin 2001; (2) Chelli et al. 1995; (3) Hughes et al. 1994; (4) Cohen 1974; (5) Meyer et al. 1993; (6) this work; (7) Greene et al. 1994; (8) Cohen & Schwartz 1983; (9) Knacke et al. 1973; (10) Walter et al. 1997; (11) Wilking et al. 1992.

Table 4. Spectral Features and Bandpasses for Equivalent Widths

| $\lambda_{central}$<br>( $\mu\text{m}$ ) | $\Delta\lambda$<br>( $\text{\AA}$ ) | Species        | Transition                            | Comments               |
|--|-------------------------------------|----------------|---------------------------------------|------------------------|
| 2.05869                                  | 120                                 | He I           | $2p^1P^o - 2s^1S$                     | $\oplus$ Contamination |
| 2.10655                                  | 85                                  | Mg I           | $4f^1F_3^o - 7g^1G_4$                 | blend                  |
| 2.10666                                  | 85                                  | Mg I           | $4f^3F_{2,3,4}^o - 7g^3G_{3,4,5}^o$   | blend                  |
| 2.10988                                  | 85                                  | Al I           | $4p^2P_{1/2}^o - 5s^2S_{1/2}$         | blend                  |
| 2.11695                                  | 75                                  | Al I           | $4p^2P_{3/2}^o - 5s^2S_{1/2}$         |                        |
| 2.12183                                  | 120                                 | H <sub>2</sub> | $\nu = 1 - 0 S(1)$                    |                        |
| 2.16611                                  | 120                                 | H I            | $n = 7 - 4 \text{ (Br}\gamma\text{)}$ |                        |
| 2.20624                                  | 70                                  | Na I           | $4p^2P_{3/2}^o - 4s^2S_{1/2}$         | blend                  |
| 2.20897                                  | 70                                  | Na I           | $4p^2P_{1/2}^o - 4s^2S_{1/2}$         | blend                  |
| 2.26141                                  | 110                                 | Ca I           | $4f^3F_2^o - 4d^3D_1$                 | blend                  |
| 2.26311                                  | 110                                 | Ca I           | $4f^3F_3^o - 4d^3D_2$                 | blend                  |
| 2.26573                                  | 110                                 | Ca I           | $4f^3F_4^o - 4d^3D_3$                 | blend                  |
| 2.28141                                  | 100                                 | Mg I           | $4d^3D_{3,2,1} - 6f^3F_{2,3,4}^o$     |                        |
| 2.29353                                  | 130                                 | CO             | $v = 2 - 0$ bandhead                  |                        |
| 2.32265                                  | 130                                 | CO             | $v = 3 - 1$ bandhead                  |                        |
| 2.35246                                  | 130                                 | CO             | $v = 4 - 2$ bandhead                  |                        |
| 2.38295                                  | 130                                 | CO             | $v = 5 - 3$ bandhead                  |                        |

Note. — For the Mg I + Al I blend at  $2.11\mu\text{m}$ ,  $\Delta\lambda$  refers to the entire blended feature. The same applies for the bandpasses of the Na I doublet ( $2.21\mu\text{m}$ ) and the Ca I triplet ( $2.26\mu\text{m}$ ) blends.

Table 5. Standard Star  $K$  band Equivalent Widths ( $\text{\AA}$ )

| Name     | Spectral Type | 2.110<br>Al I + Mg I | 2.117<br>Al I | 2.166<br>H I | 2.208<br>Na I | 2.264<br>Ca I | 2.281<br>Mg I | 2.294<br>CO(2–0) | 2.323<br>CO(3–1) | 2.352<br>CO(4–2) | 2.383<br>CO(5–3) |
|----------|---------------|----------------------|---------------|--------------|---------------|---------------|---------------|------------------|------------------|------------------|------------------|
| HR 88    | G2.5 V        | 1.7                  | 1.5           | 3.7          | 1.1           | 1.1           | 1.2           | ...              | ...              | ...              | ...              |
| HR 8631  | G4 V          | 1.1                  | 1.1           | 2.4          | 1.1           | 1.2           | 1.0           | 2.2              | 4.0              | 2.9              | 3.8              |
| HR 9088  | G5 V          | 0.7                  | 0.5           | 2.9          | 0.9           | 1.0           | 0.9           | 1.0              | 1.0              | 1.1              | 1.5              |
| HR 8784  | G8 IV         | 1.5                  | 1.6           | 2.5          | 1.3           | 1.2           | 1.2           | 4.0              | 4.2              | 5.1              | 5.2              |
| HR 166   | K0 V          | 1.3                  | 0.6           | 2.5          | 1.8           | 1.4           | 1.8           | 3.7              | 3.5              | 4.9              | 4.3              |
| GL 28    | K2 V          | 2.4                  | 2.1           | 1.3          | 2.1           | 2.7           | 2.3           | 4.4              | 5.6              | 4.9              | 5.7              |
| HR 8832  | K3 V          | 2.4                  | 1.9           | 1.1          | 2.2           | 2.9           | 1.6           | 4.0              | 4.1              | 5.0              | 6.0              |
| HR 8085  | K5 V          | 1.4                  | 1.4           | ...          | 2.2           | 2.9           | 1.1           | 4.1              | 3.8              | 4.9              | 5.2              |
| HR 8086  | K7 V          | 1.8                  | 1.8           | ...          | 3.1           | 3.5           | 1.1           | 4.8              | 5.2              | 5.3              | 5.3              |
| GL 763   | M0 V          | 1.1                  | 1.6           | ...          | 2.9           | 3.7           | 1.3           | 4.4              | 4.2              | 4.8              | 4.2              |
| GL 752.a | M3 V          | 0.9                  | 1.4           | ...          | 4.2           | 4.5           | 0.7           | 4.6              | 4.1              | 4.6              | 4.0              |
| GL 791.2 | M4.5 V        | ...                  | ...           | ...          | 4.5           | 2.6           | 0.5           | 6.3              | 4.5              | 5.7              | 4.3              |
| GL 83.1  | M5 V          | ...                  | ...           | ...          | 4.1           | 1.8           | 0.5           | 5.1              | 4.2              | 4.8              | 3.7              |
| GL 644c  | M7 V          | ...                  | ...           | ...          | 3.7           | 0.8           | 0.8           | 6.8              | 6.1              | 5.3              | 4.5              |
| GL 752.b | M8 V          | ...                  | ...           | ...          | 4.4           | 0.7           | 1.0           | 8.6              | 6.6              | 6.4              | 4.8              |

Table 6. Equivalent Widths ( $\text{\AA}$ ) of Spectroscopic Sample

| Name     |   | 2.059<br>He I | 2.110<br>Mg I + Al I | 2.117<br>Al I | 2.122<br>H <sub>2</sub> | 2.166<br>H I | 2.208<br>Na I | 2.264<br>Ca I | 2.281<br>Mg I | 2.294<br>CO(2-0) | 2.323<br>CO(3-1) | 2.352<br>CO(4-2) | 2.383<br>CO(5-3) |
|----------|---|---------------|----------------------|---------------|-------------------------|--------------|---------------|---------------|---------------|------------------|------------------|------------------|------------------|
| HBC 248  | A | ...           | 1.4                  | 1.4           | ...                     | ...          | 1.4           | 2.2           | 1.1           | 4.1              | 3.4              | 4.4              | 4.1              |
|          | B | ...           | 0.7                  | 0.7           | ...                     | ...          | 2.0           | 2.0           | 0.4           | 4.3              | 3.6              | 4.2              | 4.6              |
| HBC 620  | A | ...           | 2.1                  | 1.8           | ...                     | ...          | 3.7           | 4.6           | 1.0           | 6.5              | 4.3              | 4.4              | 5.2              |
|          | B | ...           | ...                  | ...           | ...                     | -1.54        | 1.6           | 1.4           | ...           | 3.4              | 1.1              | 3.5              | 2.4              |
| HBC 625  | A | ...           | 1.3                  | 1.5           | ...                     | ...          | 4.1           | 4.1           | 0.8           | 5.3              | 4.2              | 5.9              | 5.3              |
|          | B | ...           | 0.4                  | 0.7           | ...                     | ...          | 3.5           | 4.0           | 0.6           | 5.8              | 2.3              | 5.1              | 3.6              |
| AS 205   | A | ...           | ...                  | ...           | ...                     | -3.0         | ...           | 0.8           | ...           | ...              | ...              | ...              | ...              |
|          | B | ...           | 1.1                  | 0.8           | ...                     | -1.7         | 1.6           | 1.8           | 0.8           | 3.1              | 2.3              | 2.7              | 2.6              |
| WSB 4    | A | ...           | 1.4                  | 1.7           | ...                     | ...          | 3.6           | 4.1           | ...           | 4.9              | 2.5              | 3.6              | 2.5              |
|          | B | ...           | 1.2                  | 1.0           | ...                     | -1.0         | 1.7           | 2.6           | 0.5           | 2.7              | 2.8              | 2.3              | 1.5              |
| WSB 19   | A | ...           | 1.9                  | 1.3           | ...                     | -1.4         | 2.6           | 3.0           | 0.6           | 5.2              | 2.2              | 3.7              | 3.7              |
|          | B | ...           | 1.6                  | 1.8           | ...                     | -0.7         | 2.1           | 2.6           | 1.0           | 6.2              | ...              | 2.7              | 3.3              |
| WSB 28   | A | ...           | 0.6                  | 0.9           | ...                     | ...          | 3.8           | 4.7           | 1.6           | 7.8              | 6.3              | 6.7              | 6.2              |
|          | B | ...           | ...                  | ...           | ...                     | ...          | 0.8           | 0.7           | 0.6           | 4.7              | 4.8              | 1.9              | 3.4              |
| DoAr 24E | A | ...           | 1.3                  | 0.6           | ...                     | ...          | 1.2           | 1.4           | 0.3           | 3.9              | 2.6              | 3.6              | 3.3              |
|          | B | ...           | ...                  | ...           | ...                     | -0.9         | ...           | ...           | ...           | ...              | ...              | ...              | ...              |
| DoAr 26  | A | ...           | ...                  | ...           | ...                     | -2.2         | 2.4           | 2.1           | 0.5           | 3.6              | 1.5              | 2.7              | 2.8              |
|          | B | ...           | ...                  | ...           | ...                     | ...          | 2.4           | 3.1           | 1.0           | 5.1              | 3.1              | 2.8              | 4.3              |
| ROX 15   | A | ...           | 1.5                  | 1.4           | ...                     | ...          | 2.4           | 2.8           | 0.8           | 5.7              | 4.4              | 4.6              | 5.1              |
|          | B | ...           | 1.1                  | 1.7           | ...                     | ...          | 2.3           | 2.8           | 0.9           | 6.3              | 4.1              | 2.2              | 4.8              |
| SR 21    | A | ...           | 0.7                  | 0.5           | ...                     | 2.1          | 0.5           | ...           | 0.5           | ...              | ...              | ...              | ...              |
|          | B | ...           | 1.2                  | 0.8           | ...                     | ...          | 3.4           | 3.6           | ...           | 6.3              | 5.5              | 4.7              | 5.5              |

Table 6—Continued

|            |   | 2.059 | 2.110       | 2.117 | 2.122          | 2.166 | 2.208 | 2.264 | 2.281 | 2.294   | 2.323   | 2.352   | 2.383   |
|------------|---|-------|-------------|-------|----------------|-------|-------|-------|-------|---------|---------|---------|---------|
| Name       |   | He I  | Mg I + Al I | Al I  | H <sub>2</sub> | H I   | Na I  | Ca I  | Mg I  | CO(2-0) | CO(3-1) | CO(4-2) | CO(5-3) |
| YLW 15A    | A | ...   | ...         | ...   | ...            | −1.3  | 0.7   | 0.9   | ...   | ...     | ...     | ...     | ...     |
|            | B | ...   | ...         | ...   | ...            | ...   | ...   | ...   | ...   | ...     | ...     | ...     | ...     |
| WSB 71     | A | ...   | 1.0         | 0.8   | ...            | ...   | 1.4   | 1.3   | 0.9   | 2.4     | 2.6     | 1.8     | 2.5     |
|            | B | ...   | ...         | ...   | ...            | −1.8  | 2.9   | 3.2   | ...   | 6.5     | 4.6     | 4.2     | 5.5     |
| S CrA      | A | ...   | ...         | ...   | ...            | −3.9  | ...   | 0.9   | ...   | 0.9     | 0.5     | 1.1     | 0.9     |
|            | B | ...   | ...         | ...   | ...            | −2.8  | ...   | 0.8   | ...   | 1.3     | 0.5     | 1.1     | 1.0     |
| HBC 679    | A | ...   | 2.1         | 1.7   | ...            | ...   | 3.5   | 4.5   | 1.8   | 4.5     | 4.3     | 5.0     | 4.5     |
|            | B | ...   | 1.9         | 1.4   | ...            | ...   | 3.6   | 3.7   | ...   | 3.5     | 3.5     | 2.3     | 2.6     |
| VV CrA '96 | A | −2.1  | ...         | ...   | ...            | −15.7 | −0.6  | 2.0   | ...   | −5.0    | −4.1    | −2.3    | −1.4    |
|            | B | ...   | ...         | ...   | −0.5           | −3.5  | −0.5  | 0.7   | ...   | −2.3    | −2.2    | −1.3    | −1.3    |
| VV CrA '97 | A | −1.3  | 0.5         | 0.2   | −0.8           | −14.2 | −0.8  | 1.7   | ...   | −4.8    | −2.9    | −2.6    | −1.3    |
|            | B | ...   | ...         | ...   | −2.1           | −4.0  | −0.4  | 0.7   | ...   | −2.1    | −1.5    | −2.2    | −1.1    |
| AS 353     | A | ...   | 0.6         | 0.6   | ...            | −21.1 | −1.0  | 1.2   | ...   | −2.4    | −0.2    | −0.8    | ...     |
|            | B | ...   | 1.5         | 1.6   | ...            | ...   | 2.0   | 3.1   | 0.9   | 6.2     | 6.1     | 4.9     | 5.8     |

Table 7. Derived Sample Properties

| Name     |   | Spectral<br>Type <sup>c</sup> | $T_{eff}^a$<br>(K) | $A_V$<br>(mag) | $r_k$<br>( $F_{K_{ex}}/F_{K*}$ ) | $d^b$<br>(pc)                     | $L_*$<br>( $L_\odot$ )                   | Reference<br>(d) |
|----------|---|-------------------------------|--------------------|----------------|----------------------------------|-----------------------------------|--|------------------|
| HBC 248  | A | K2 (1)                        | 4900±150           | 4.0±0.9        | 0.10±0.11                        | 159 <sup>+77</sup> <sub>-39</sub> | 14.49 <sup>+17.44</sup> <sub>-6.23</sub> | 1                |
|          | B | M6 (1)                        | 3000±150           | 0.0±1.1        | 0.07±0.18                        | 159 <sup>+77</sup> <sub>-39</sub> | 0.29 <sup>+0.35</sup> <sub>-0.12</sub>   | 1                |
| HBC 620  | A | M0 (1)                        | 3800±200           | 0.4±1.1        | 0.00±0.12                        | 150                               | 0.68 <sup>+0.19</sup> <sub>-0.17</sub>   | 2                |
|          | B | M4.5(1)                       | 3200±150           | 0.5±1.4        | 0.03±0.17                        | 150                               | 0.08±0.02                                | 2                |
| HBC 625  | A | M1.5(1)                       | 3650±150           | 0.0±0.8        | 0.00±0.08                        | 150                               | 0.22±0.06                                | 2                |
|          | B | M4 (1)                        | 3250±150           | 0.9±0.7        | 0.03±0.08                        | 150                               | 0.11±0.03                                | 2                |
| AS 205   | A | K5 (2)                        | 4450±400           | 2.9±1.3        | 2.35±0.87                        | 160                               | 7.10 <sup>+1.89</sup> <sub>-1.66</sub>   | 3                |
|          | B | M3 (2)                        | 3450±300           | 2.1±1.0        | 0.72±0.15                        | 160                               | 2.19 <sup>+0.58</sup> <sub>-0.51</sub>   | 3                |
| WSB 4    | A | M3 (2)                        | 3450±300           | 0.0±1.0        | 0.00±0.11                        | 160                               | 0.11±0.03                                | 3                |
|          | B | M3 (1)                        | 3450±150           | 0.4±1          | 0.19±0.10                        | 160                               | 0.15±0.04                                | 3                |
| WSB 19   | A | M3 (1)                        | 3450±150           | 1.7±1          | 0.37±0.07                        | 160                               | 0.29±0.08                                | 3                |
|          | B | M5 (1)                        | 3150±150           | 2.7±1.4        | 0.00±0.15                        | 160                               | 0.18±0.05                                | 3                |
| WSB 28   | A | M3 (1)                        | 3450±150           | 5.1±0.6        | 0.00±0.06                        | 160                               | 0.69 <sup>+0.18</sup> <sub>-0.16</sub>   | 3                |
|          | B | M7 (1)                        | 2850±150           | 2.5±1          | 0.14±0.10                        | 160                               | 0.04±0.01                                | 3                |
| DoAr 24E | A | K0 (3)                        | 5250±400           | 5.7±1.0        | 0.25±0.12                        | 160                               | 8.78 <sup>+2.33</sup> <sub>-2.05</sub>   | 3                |
|          | B | ...                           | ...                | ...            | ...                              | ...                               | ...                                      |                  |
| DoAr 26  | A | M4 (1)                        | 3250±150           | 3.3±1.2        | 0.98±0.49                        | 160                               | 0.36 <sup>+0.10</sup> <sub>-0.08</sub>   | 3                |
|          | B | M6 (1)                        | 3000±150           | 1.0±0.9        | 0.14±0.10                        | 160                               | 0.11±0.03                                | 3                |
| ROX 15   | A | M3 (2)                        | 3450±300           | 11.1±0.8       | 0.06±0.09                        | 160                               | 3.45 <sup>+0.92</sup> <sub>-0.81</sub>   | 3                |
|          | B | M3 (2)                        | 3450±300           | 13.8±1.1       | 0.22±0.13                        | 160                               | 1.35 <sup>+0.36</sup> <sub>-0.32</sub>   | 3                |
| SR 21    | A | G2.5 (3)                      | 5950±300           | 9.0±0.9        | 0.78±0.54                        | 160                               | 28.04 <sup>+7.45</sup> <sub>-6.57</sub>  | 3                |
|          | B | M4 (1)                        | 3250±150           | 9.3±1.1        | 0.15±0.11                        | 160                               | 0.66 <sup>+0.18</sup> <sub>-0.16</sub>   | 3                |
| YLW 15A  | A | K2 (3)                        | 4900±500           | 38±4           | 1.7±0.5                          | 160                               | 11.40 <sup>+3.03</sup> <sub>-2.67</sub>  | 3                |
|          | B | ...                           | ...                | ...            | ...                              | ...                               | ...                                      |                  |
| WSB 71   | A | K2 (3)                        | 4900±500           | 8.0±0.7        | 1.12±0.30                        | 160                               | 2.30 <sup>+0.61</sup> <sub>-0.54</sub>   | 3                |
|          | B | M6 (2)                        | 3000±300           | 4.7±1.0        | 0.05±0.12                        | 160                               | 0.34±0.09                                | 3                |
| S CrA    | A | K3 (2)                        | 4800±400           | 1.0±1.0        | 2.89±1.60                        | 130                               | 2.29 <sup>+0.76</sup> <sub>-0.65</sub>   | 5                |
|          | B | M0 (2)                        | 3800±400           | 1.0±1.0        | 3.15±2.00                        | 130                               | 0.76 <sup>+0.25</sup> <sub>-0.22</sub>   | 5                |
| HBC 679  | A | K5 (3)                        | 4450±500           | 4.8±0.7        | 0.00±0.07                        | 130                               | 0.87 <sup>+0.29</sup> <sub>-0.25</sub>   | 5                |
|          | B | M3 (1)                        | 3450±150           | 1.6±1.0        | 0.00±0.10                        | 130                               | 0.05±0.02                                | 5                |

Table 7—Continued

| Name   | Spectral<br>Type <sup>c</sup> | $T_{eff}$ <sup>a</sup><br>(K) | $A_V$<br>(mag) | $r_k$<br>( $F_{K_{ex}}/F_{K_*}$ ) | $d$ <sup>b</sup><br>(pc) | $L_*$<br>( $L_\odot$ )  | Reference<br>(d) |
|--------|-------------------------------|-------------------------------|----------------|-----------------------------------|--------------------------|-------------------------|------------------|
| AS 353 | A ...                         | ...                           | ...            | ...                               | ...                      | ...                     |                  |
|        | B M3 (2)                      | 3450±300                      | 2.1±0.8        | 0.02±0.08                         | 150±50                   | 0.68 $^{+0.52}_{-0.38}$ | 4                |

<sup>a</sup>Spectral type to  $T_{eff}$  conversions estimated from scale provided in Figure 5 of Luhman (2000).

<sup>b</sup>Distance was not a derived quantity but is included here to show what values were used in the calculation of  $L_*$ . The uncertainty is  $\pm 20$ pc unless otherwise noted.

<sup>c</sup>The approximate uncertainty in the derived spectral type is given in parenthesis, in units of spectral subclasses.

References. — (1) Perryman et al. 1997; (2) Krautter et al. 1991; (3) de Geus et al. 1989; (4) Edwards & Snell 1982; (5) Marraco & Rydgren 1981.

Table 8. Component Ages and Masses

| Name          |   | Age <sup>a</sup><br>(yrs) | $M^b$<br>( $M_{\odot}$ ) | $q$<br>( $M_2/M_1$ ) | Coeval<br>to $1\sigma$ ? |
|---------------|---|---------------------------|--------------------------|----------------------|--------------------------|
| HBC 248       | A | $1 \times 10^5$           | 2.5                      | 0.04                 | Y                        |
|               | B | $2 \times 10^5$           | 0.1                      |                      |                          |
| HBC 620       | A | $1 \times 10^6$           | 0.6                      | 0.25                 | Y                        |
|               | B | $2 \times 10^6$           | 0.15                     |                      |                          |
| HBC 625       | A | $3 \times 10^6$           | 0.4                      | 0.38                 | Y                        |
|               | B | $1.5 \times 10^6$         | 0.15                     |                      |                          |
| AS 205        | A | $1 \times 10^5$           | 1.5                      | 0.20                 | Y                        |
|               | B | $< 1 \times 10^5$         | 0.3                      |                      |                          |
| WSB 4         | A | $3 \times 10^6$           | 0.3                      | 1.0                  | Y                        |
|               | B | $3 \times 10^6$           | 0.3                      |                      |                          |
| WSB 19        | A | $1 \times 10^6$           | 0.3                      | 0.5                  | Y                        |
|               | B | $5 \times 10^5$           | 0.15                     |                      |                          |
| WSB 28        | A | $4 \times 10^5$           | 0.3                      | $\sim 0.2$           | Y                        |
|               | B | $\sim 1 \times 10^{6c}$   | $\sim 0.06^c$            |                      |                          |
| DoAr 24E      | A | $1.5 \times 10^6$         | $\sim 2.3$               | ...                  | ...                      |
|               | B | ...                       | ...                      |                      |                          |
| DoAr 26       | A | $4 \times 10^5$           | 0.15                     | 0.67                 | Y                        |
|               | B | $5 \times 10^5$           | 0.1                      |                      |                          |
| ROX 15        | A | $< 1 \times 10^5$         | 0.3                      | 1.0                  | Y                        |
|               | B | $1 \times 10^5$           | 0.3                      |                      |                          |
| SR 21         | A | $1 \times 10^6$           | 2.5                      | 0.06                 | N                        |
|               | B | $1 \times 10^5$           | 0.15                     |                      |                          |
| YLW 15A       | A | $1 \times 10^5$           | 2.5                      | ...                  | ...                      |
|               | B | ...                       | ...                      |                      |                          |
| H $\alpha$ 71 | A | $5 \times 10^6$           | 1.5                      | 0.07                 | N                        |
|               | B | $2 \times 10^5$           | 0.1                      |                      |                          |
| S CrA         | A | $3 \times 10^6$           | 1.5                      | 0.40                 | Y                        |
|               | B | $1 \times 10^6$           | 0.6                      |                      |                          |
| HBC 679       | A | $7 \times 10^6$           | 1.2                      | 0.25                 | Y                        |
|               | B | $1.5 \times 10^7$         | 0.3                      |                      |                          |

Table 8—Continued

| Name   |   | Age <sup>a</sup><br>(yrs) | $M^b$<br>( $M_\odot$ ) | $q$<br>( $M_2/M_1$ ) | Coeval<br>to 1 $\sigma$ ? |
|--------|---|---------------------------|------------------------|----------------------|---------------------------|
| AS 353 | A | ...                       | ...                    | ...                  | ...                       |
|        | B | $5 \times 10^5$           | 0.3                    |                      |                           |

<sup>a</sup>Typical uncertainties in age estimates range from 50–200 %.

<sup>b</sup>Typical uncertainties in mass estimates are 0.1–0.3  $M_\odot$ .

<sup>c</sup>Estimated from position on the evolutionary tracks of Baraffe et al. (1998), which appear to be roughly consistent with the extrapolation of the Palla & Stahler (1999) tracks for this location.

Table 9. Circumstellar Disk Diagnostics

| Name          |   | $F(Br\gamma)^a$<br>(W m <sup>-2</sup> )         | Dereddened $K - L$<br>(mag) | Comments                          |
|---------------|---|---|-----------------------------|-----------------------------------|
| HBC 248       | A | ...   | 0.32 ±0.15                  |                                   |
|               | B | ...   | 0.48 ±0.18                  |                                   |
| HBC 620       | A | ...   | 0.07 ±0.17                  | unresolved color                  |
|               | B | $3.09 \times 10^{-18} \pm 2.00 \times 10^{-18}$ |                             | chromospheric ?                   |
| HBC 625       | A | ...   | 0.07 ±0.09                  | unresolved color                  |
|               | B | ...   |                             |                                   |
| AS 205        | A | $7.19 \times 10^{-16} \pm 2.43 \times 10^{-16}$ | 0.83 ±0.16                  |                                   |
|               | B | $1.53 \times 10^{-16} \pm 0.90 \times 10^{-16}$ | 0.98 ±0.19                  |                                   |
| WSB 4         | A | ...   | 0.44 ±0.18                  |                                   |
|               | B | $2.87 \times 10^{-18} \pm 2.87 \times 10^{-18}$ | 0.96 ±0.18                  |                                   |
| DoAr 24E      | A | ...   | 0.40 ±0.19                  |                                   |
|               | B | $2.26 \times 10^{-17} \pm 2.41 \times 10^{-17}$ | 2.2 ±0.1                    | A <sub>V</sub> unknown            |
| ROX 15        | A | ...   | 0.13 ±0.19                  | unresolved color                  |
|               | B | ...   |                             |                                   |
| SR 21         | A | absorption                                      | 0.64 ±0.12                  |                                   |
|               | B | ...   | -0.09 ±0.14                 |                                   |
| YLW 15        | A | $1.56 \times 10^{-15} \pm 1.20 \times 10^{-15}$ | 0.86 ±0.12                  | A <sub>V</sub> =38 mag (see text) |
|               | B | ...   | 1.69 ±0.08                  | A <sub>V</sub> unknown            |
| WSB 71        | A | ...   | 1.14 ±0.21                  |                                   |
|               | B | $1.23 \times 10^{-17} \pm 0.68 \times 10^{-17}$ | 0.37 ±0.24                  | chromospheric ?                   |
| S CrA         | A | $4.23 \times 10^{-16} \pm 1.10 \times 10^{-16}$ | 1.44 ±0.13                  |                                   |
|               | B | $1.59 \times 10^{-16} \pm 0.57 \times 10^{-16}$ | 1.14 ±0.15                  |                                   |
| HBC 679       | A | ...   | -0.33 ±0.14                 | unresolved color                  |
|               | B | ...   |                             |                                   |
| VV CrA (1996) | A | $8.07 \times 10^{-16} \pm 0.52 \times 10^{-16}$ | 0.99 ±0.06                  | A <sub>V</sub> unknown            |
|               | B | $1.70 \times 10^{-16} \pm 0.49 \times 10^{-16}$ | 3.63 ±0.06                  | A <sub>V</sub> unknown            |
| VV CrA (1997) | A | $7.33 \times 10^{-16} \pm 0.52 \times 10^{-16}$ | 0.99 ±0.06                  | A <sub>V</sub> unknown            |
|               | B | $1.93 \times 10^{-16} \pm 0.49 \times 10^{-16}$ | 3.63 ±0.06                  | A <sub>V</sub> unknown            |
| AS 353        | A | $4.51 \times 10^{-16} \pm 0.21 \times 10^{-16}$ | 1.88 ±0.03                  | A <sub>V</sub> unknown            |
|               | B | ...   | 0.43 ±0.13                  |                                   |

Table 9—Continued

| Name | $F(Br\gamma)^a$<br>(W m <sup>-2</sup> ) | Dereddened $K - L$<br>(mag) | Comments |
|------|---|-----------------------------|----------|
|------|---|-----------------------------|----------|

<sup>a</sup>The uncertainty in the Br  $\gamma$  emission line flux is based on a 1 Å uncertainty in the measured equivalent width.

Fig. 1.—  $K$ -band spectra of main-sequence spectral type standards. The resolution is 760. The stars are identified in Table 2. Major spectral features are indicated; details of these transitions appear in Table 3.

Fig. 2.—  $K$ -band spectra of sample objects. The resolution is 760. The stars are identified in Table 1. Major spectral features are indicated at the top of each column of spectra; the positions of the He I and H<sub>2</sub> lines are indicated on the 1996 AS 353 and VV CrA spectra. For each system, the primary star spectrum is plotted above the secondary. All spectra were normalized to unity at 2.2  $\mu$ m and offset by an additive constant for presentation purposes. The scaling does not necessarily reflect true flux ratios.

Fig. 3.— The  $J - H$ ,  $H - K$  color-color diagram of the young star sample, excepting YLW 15A. The dash-dot line delineates between objects with (right hand side) and without a near-IR excess above photospheric values for colors, attributable to circumstellar material. The dwarf and giant star loci are overplotted. An  $A_V = 10$  reddening vector and the CTTs locus of Meyer et al. (1997) and are indicated; to the left of the dash-dot line, this locus is representative of WTTS, which have main-sequence dwarf colors.

Fig. 4.— The sum of the Na I + Ca I *versus* the CO(2–0) + CO(4–2) equivalent widths. The solid line shows the main-sequence (dwarf) locus, and the dashed line the giant locus. These loci are fits to the dwarf data, given in Table 5, and to the giant star equivalent widths calculated from the smoothed spectra of Wallace & Hinkle (1997).  $1\sigma$  errors for the fit of the loci to the stellar data are shown as dotted lines. The PMS binary components are plotted as solid squares.

Fig. 5.— Contour plot of reduced  $\chi^2$  for a range of values of  $A_v$  and  $k$  calculated for the fit of the ROX 15 secondary to the M3 standard, for a given value of the constant,  $c$ .

Fig. 6.—  $T_{eff}$  and luminosity for the young star binary components plotted on the PMS evolutionary tracks of Palla & Stahler (1999) and Baraffe et al. (1998). The young star sample is plotted in the upper panels; the open symbols represent objects in the Ophiuchus SFR. Primary stars are plotted as squares and secondaries as triangles. A sample of main-sequence spectral type standard stars appears in the lower panels. The mass tracks and isochrones are labelled in the lower panels. For objects lying between labelled isochrones and mass tracks, the ages and masses were estimated by interpolation.

Fig. 7.— Same as the upper, left hand panel in Figure 6 except each binary pair is plotted individually, as labelled. The mass tracks and isochrones are the same as labelled in Figure 6, lower left hand panel.

Fig. 8.— Histogram of  $M_2/M_1$  for the 13 systems with measured masses for both components. The  $q = 0$  bin contains one object with  $q < 0.05$ .

Fig. 9.— Mass ratio as a function of binary separation. Uncertainties in the mass ratios are not shown but are as high as  $\sim 100\%$  in a few cases. Nonetheless, a trend towards lower mass ratios at larger separations appears to be present.

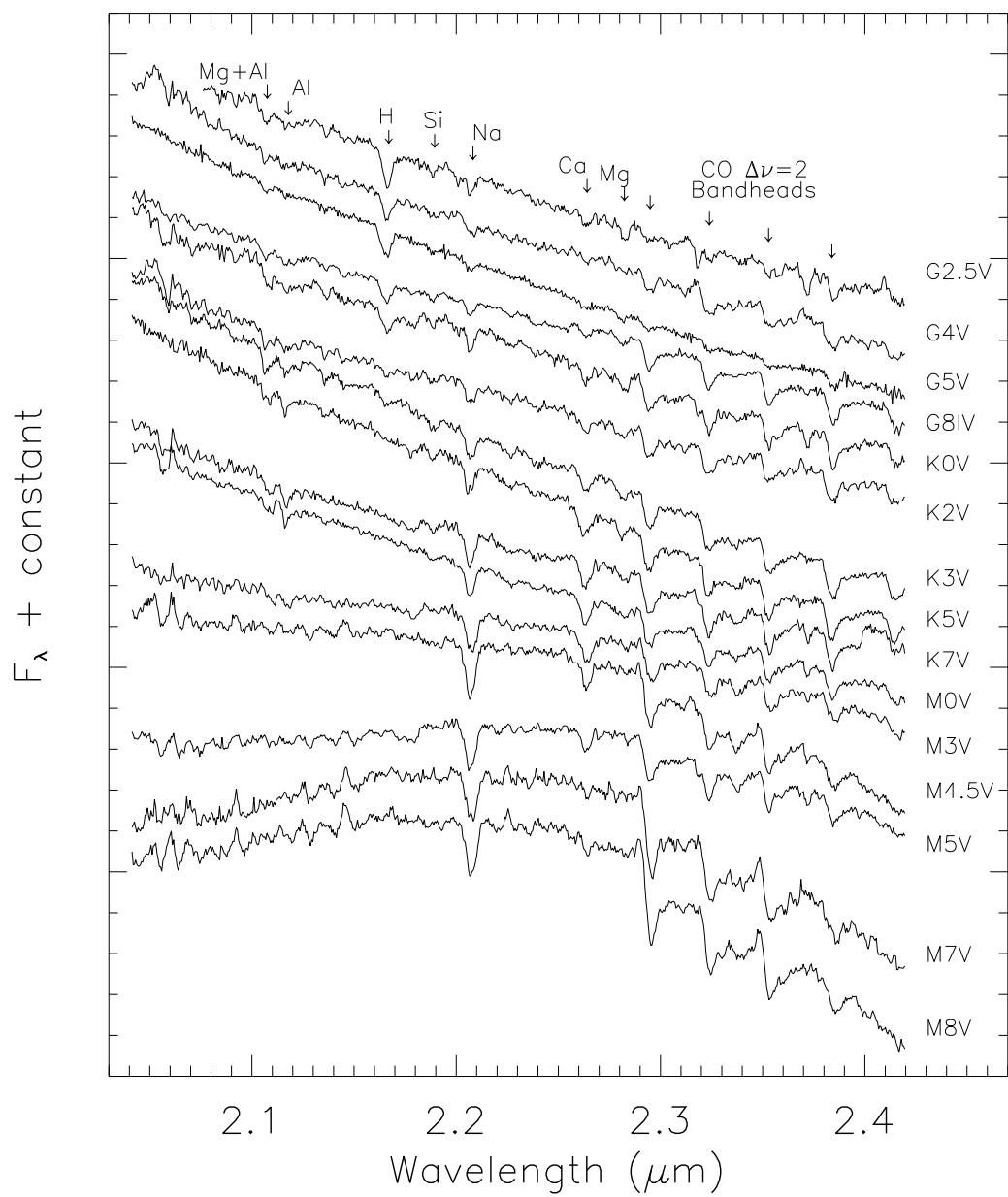
Fig. 10.— The primary *versus* secondary  $A_v$ 's for all the stars in the spectroscopic sample except the components in DoAr 24 E, YLW 15 A, VV CrA, and AS 353. A typical  $\pm 1$  mag error bar is shown in the lower right hand corner. The dotted line delineates equal component extinctions.

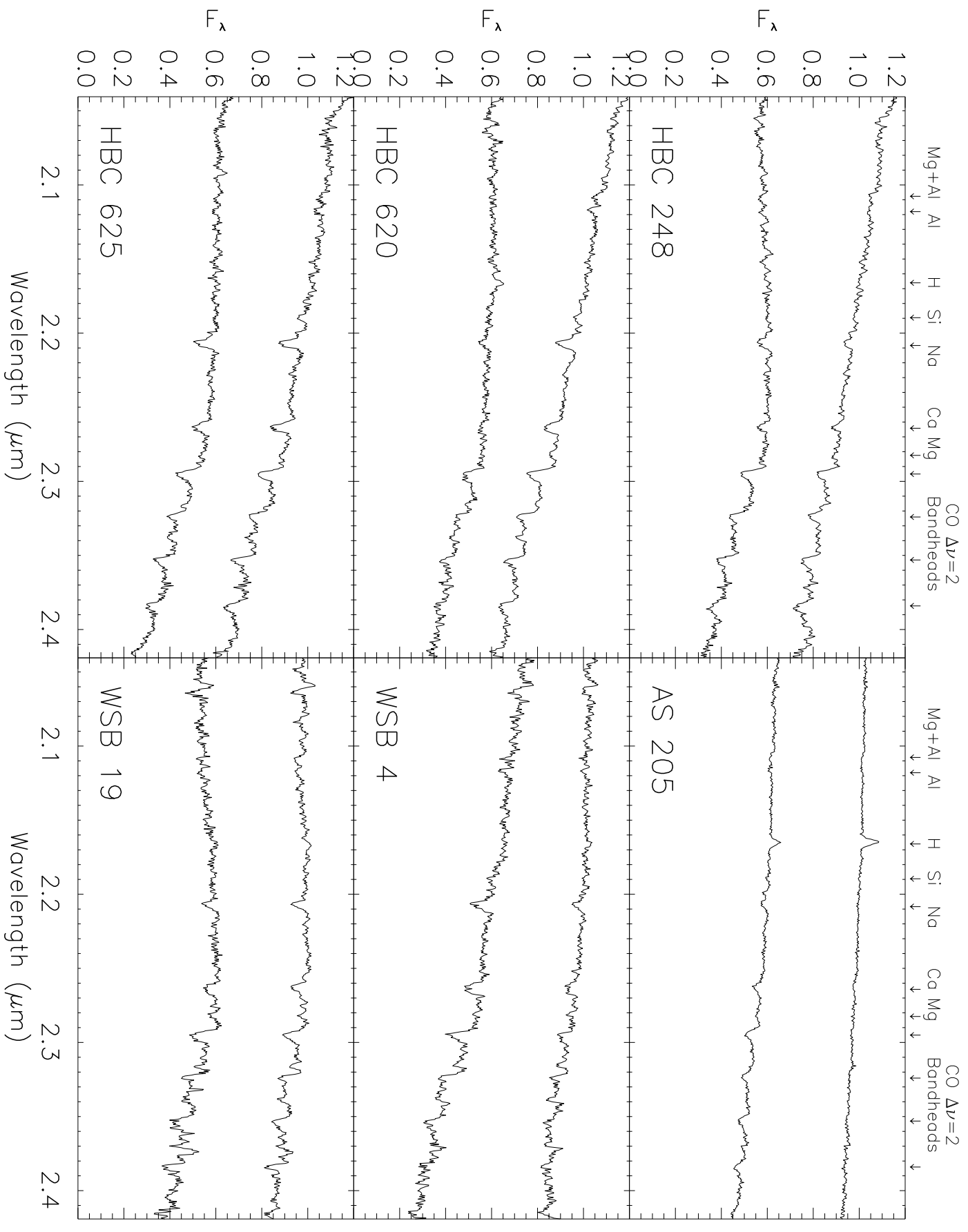
Fig. 11.— The primary *versus* secondary  $K - L$  colors as available for the sample objects (Table 9). *Open triangles*: systems for which both components have been dereddened. *Filled squares*: Systems for which it was not possible to deredden both components; the letters next to each symbol indicate which component was *not* dereddened: primary (P), secondary (S), or both (B). A typical uncertainty is shown in the lower right hand corner. The dashed line delineates equal component  $K - L$  colors. The dotted line shows the upper limit of the CTT/WTT 0.4 mag cutoff of Edwards et al. (1993) (see also §4.3.1).

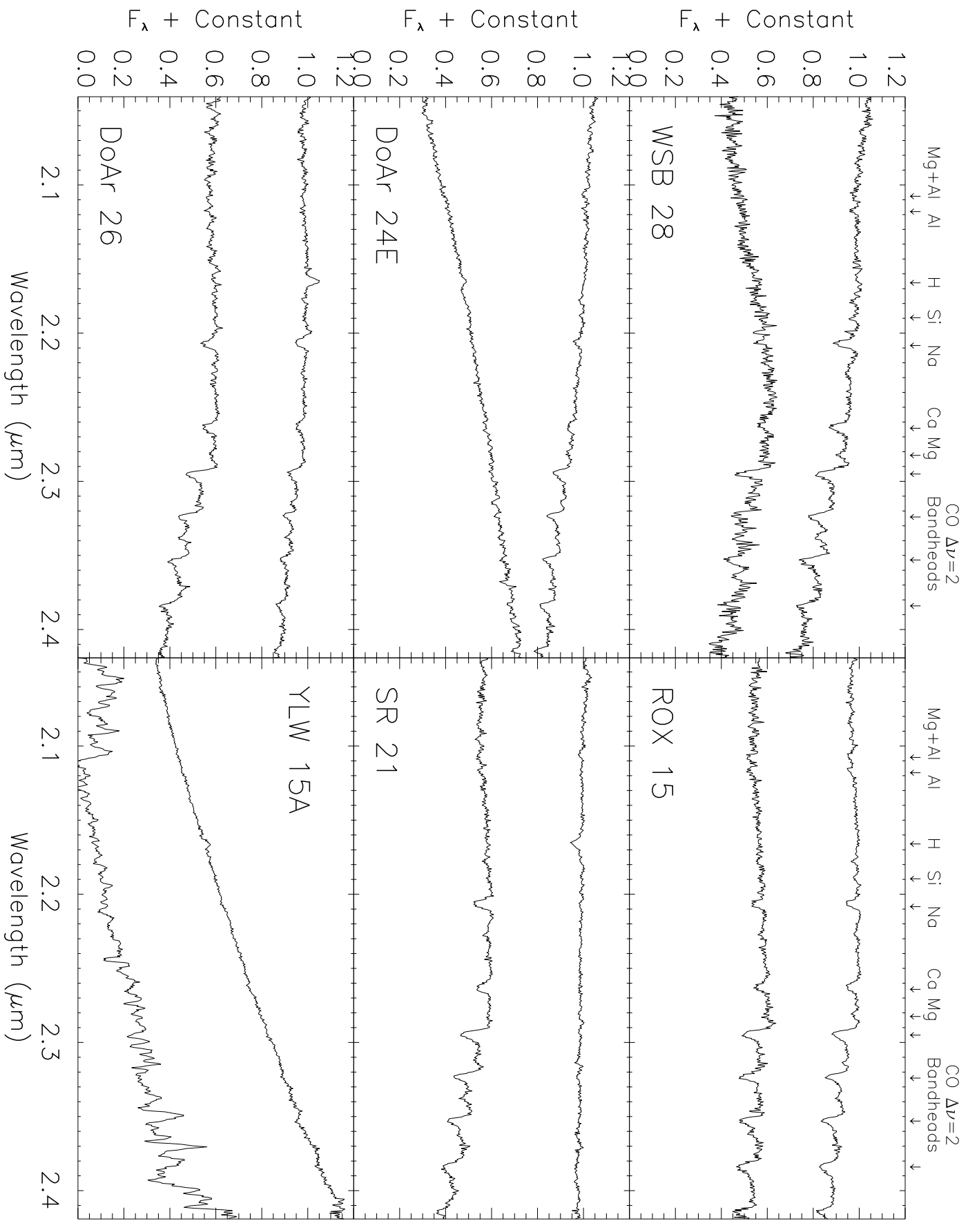
Fig. 12.— The primary *versus* secondary  $r_k$  veiling parameter for the objects as described in the Figure 10 caption. The dashed line delineates equal component  $r_k$  values. The dotted lines indicate probable cutoff between objects with and without a  $K$ -band excess.

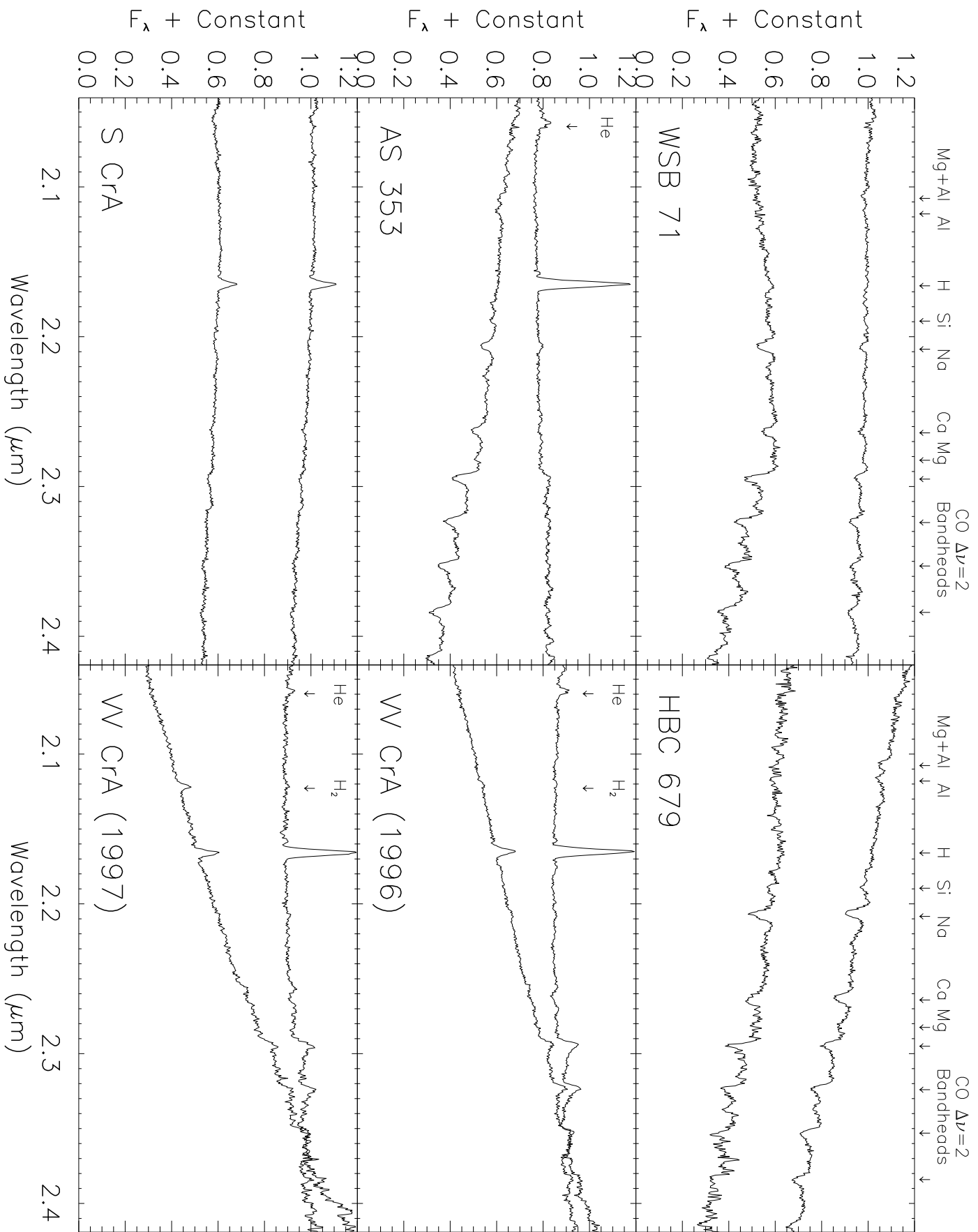
Fig. 13.— The  $K$ -band excess,  $r_k$ , plotted as a function of the  $K - L$  color of the star. In several cases, where component resolved  $K - L$  colors of the systems were not available, we plot the  $K - L$  total for the system and the higher of the  $r_k$  values for the two stars (Table 7). These are designated with an open triangle. The dot-dash and dotted lines represent the cutoffs in the respective quantities for CTT *versus* WTT behavior.

Fig. 14.— The spectrum of YLW 15A, unextinguished by  $A_V = 3.8$ , with a  $K$ -band excess of 1.7 subtracted, and smoothed by a boxcar of width 5 pixels ( $\sim 1$  resolution element). The lower spectrum is that of a K2 standard star. The observed spectrum of YLW 15A appears in Figure 2.









Near-IR Color-Color Diagram

